The Journal of Chemical Physics ARTICLE pubs.aip.org/aip/jcp

Benchmark assessment of collinear, mixed-reference, and spin-adapted variants of spin-flip time-dependent density functional theory, for closed- and open-shell molecules

Cite as: J. Chem. Phys. 164, 174102 (2026); doi: 10.1063/5.0327478
Submitted: 11 February 2026 • Accepted: 2 April 2026 •
Published Online: 4 May 2026

Avik Kumar Ojha and John M. Herbert[a)]

AFFILIATIONS

Department of Chemistry and Biochemistry, The Ohio State University, Columbus, Ohio 43210, USA

[a)]Author to whom correspondence should be addressed: herbert@chemistry.ohio-state.edu

ABSTRACT

Spin-flip methods provide access to certain electronic states having multireference character while retaining single-reference cost. However, conventional spin-flip time-dependent density functional theory (SF-TDDFT) often suffers from severe spin contamination that may cause inaccurate state ordering or engender ambiguous state character. For singlet excited states, this is largely rectified by a "mixed-reference" formulation (MRSF-TDDFT), while a spin-adapted formalism (SA-SF-TDDFT) addresses spin contamination in a general way for arbitrary multiplicities. Here, we revisit SA-SF-TDDFT and demonstrate that it significantly improves the agreement with reference data compared to other variants and also relative to conventional (spin-conserving) linear response TDDFT. Overall, SA-SF-TDDFT proves to be the most accurate among these methods, for excitation energies of both closed-shell molecules and doublet radicals as well as for singlet–triplet gaps. However, SF methods exhibit a notable limitation in the case of linear and quasi-linear doublet radicals, due to degeneracies in the high-spin quartet reference state.

I. INTRODUCTION

Accurate prediction of electronic excitation energies is essential for understanding photochemical and photophysical processes in molecular systems. Among modern electronic structure approaches, time-dependent density functional theory (TDDFT) often strikes a useful balance between cost and accuracy,[1,2] although it cannot correctly describe conical intersections involving the ground state.[3–7] Especially for photochemical applications, methods based on spin-flip (SF-)TDDFT have thus emerged as alternatives.[6–10] SF-TDDFT has been used to optimize conical intersections,[6,11–15] to determine excited-state reaction pathways,[15–17] and to perform nonadiabatic molecular dynamics simulations.[18–21] By using a sacrificial reference state of higher multiplicity (total spin $S+1$) compared to the target multiplicity (spin S), SF-TDDFT puts the spin-S ground state into the variational space where it is optimized alongside excited states of the same multiplicity. This resolves problems with the description of conical intersections involving the ground state.[6,7,20]

A major strength of SF-TDDFT lies in its ability to access states with multiconfigurational character, such as diradicals and bond-breaking geometries.[8,22,23] It does so by including a limited set of doubly substituted determinants that are absent in conventional (spin-conserving) linear-response (LR-)TDDFT.[7] Omission of double excitations is the reason why conventional single-reference methods fail qualitatively in situations involving near-degeneracy.[3–5] SF-TDDFT incorporates the most important doubles in an automated way that does not increase the asymptotic scaling of the method, which remains $\mathcal{O}(N^4)$ with system size.[6,7]

A persistent limitation of SF-TDDFT is spin contamination.[15] This arises because many of the spin-flipped determinants lack their corresponding "spin complements,"[7,24] resulting in states that are not spin eigenfunctions. This significantly complicates state-tracking in excited-state optimizations and molecular dynamics, where states with different diabatic character and multiplicity cross and mix as the molecule moves along a potential energy surface.

To overcome this drawback, spin-adapted (SA-)SF methods have been developed[24–29] based on the tensor equation-of-motion formalism.[30] This approach constructs a spin-complete set of excitation operators so that the excited-state wave functions are necessarily $\hat{S}^2$ eigenstates. The configuration-interaction singles (CIS) version of this approach[24] generalizes the SF-CIS model.[22] Borrowing ideas from the DFT/CIS method,[31–33] Kohn–Sham (KS) orbitals can be used as a low-cost means to include dynamic electron correlation. The result is SA-SF-TDDFT,[24] a hybrid method that includes electron correlation (for quantitative description of excitation energies) while properly describing conical intersections with the ground state, all within a model that is rigorously free of spin contamination and similar in cost to LR-TDDFT.

While there have been some previous assessments of the accuracy of SF-TDDFT for vertical excitation energies,[34–40] there has not yet been a comprehensive side-by-side comparison of different variants of this approach. The present work seeks to assess SA-SF-TDDFT in comparison with SF-TDDFT and also with a "mixed reference" variant (MRSF-TDDFT),[10,23,39–43] which is significantly less afflicted by spin contamination compared to conventional SF-TDDFT.[41] We also report traditional LR-TDDFT calculations with several popular functionals in order to establish a baseline for closed-shell systems where this approach performs well.[1] The performance of unrestricted TDDFT for open-shell species is less favorable,[44] and is compared alongside SF- and SA-SF-TDDFT in the present work.

These assessments primarily rely on the "QUEST" database,[45] a large collection of theoretical best estimates (TBEs) for vertical excitation energies, derived from high-level *ab initio* calculations. This database spans a diverse set of valence, Rydberg, and charge-transfer (CT) excitations and provides a standard that does not require extraction of vertical excitation energies from experimental spectra that include vibrational averaging or, conversely, simulation of vibrational structure in the theoretical spectrum. Separately, we will also consider vertical transition energies in some diradicals and in a set of molecules with inverted singlet–triplet gaps.[46]

The SF-TDDFT methods examined here are all "collinear" formulations of the method, in which the direction of the magnetization vector is the same at every point in space.[47,48] There is some evidence that relativistic,[49–51] non-collinear variants[52–57] of SF-TDDFT may afford better excitation energies,[9,56,58] especially for functionals with a low fraction of Hartree–Fock exchange (HFX).[36,37] However, the non-collinear formulation is subject to numerical instabilities in cases of rapidly varying spin polarization.[9,35,55–60] Although there are workarounds,[35,60] these are not without problems.[57] While there has been some recent methodological progress on resolving this issue,[48,61] the present work is restricted to collinear SF-TDDFT.

II. THEORY

We first present a brief overview of LR-TDDFT (Sec. II A),[1,62] as a foundation for introducing collinear SF-TDDFT (Sec. II B).[8] This is followed by the introduction of MRSF-TDDFT in Sec. II C[10] and then SA-SF-TDDFT in Sec. II D.[24] A pedagogical introduction to LR-TDDFT can be found in Ref. 1, and a similarly didactic overview of SF-TDDFT variants can be found in Ref. 7.

A. LR-TDDFT

The ground-state KS equation is

$$\hat{F}\psi_{p\sigma}(\mathbf{r}) = \varepsilon_{p\sigma}\psi_{p\sigma}(\mathbf{r}), \tag{1}$$

which defines the molecular orbitals (MOs) $\{\psi_{p\sigma}\}$, where $\sigma \in \{\alpha,\beta\}$ is a spin index. LR-TDDFT corresponds to the excited-state eigenvalue problem

$$\begin{bmatrix} \mathbf{A} & \mathbf{B} \\ \mathbf{B}^* & \mathbf{A}^* \end{bmatrix}\begin{bmatrix} \mathbf{x} \\ \mathbf{y} \end{bmatrix} = \omega\begin{bmatrix} \mathbf{1} & \mathbf{0} \\ \mathbf{0} & -\mathbf{1} \end{bmatrix}\begin{bmatrix} \mathbf{x} \\ \mathbf{y} \end{bmatrix}, \tag{2}$$

where ω denotes the excitation energy and vectors $\mathbf{x}$ and $\mathbf{y}$ represent excitation and de-excitation amplitudes, respectively.[62] (See Ref. 1 for a pedagogical introduction.) Orbital Hessians $\mathbf{A}$ and $\mathbf{B}$ have matrix elements

$$A_{ia\sigma,jb\sigma'} = \delta_{ij}\delta_{ab}\delta_{\sigma\sigma'}(\varepsilon_a - \varepsilon_i) + \frac{\partial F_{ia\sigma}}{\partial P_{jb\sigma'}}, \tag{3a}$$

$$B_{ia\sigma,jb\sigma'} = \frac{\partial F_{ia\sigma}}{\partial P_{bj\sigma'}}. \tag{3b}$$

In more detail, the matrix elements of $\mathbf{A}$ are

$$\begin{aligned} A_{ia\sigma,jb\sigma'} = {} & (\varepsilon_a - \varepsilon_i)\delta_{ia}\delta_{jb}\delta_{\sigma\sigma'} + (ia|jb) - c_{\mathrm{hfx}}(ij|ab)\delta_{\sigma\sigma'} \\ & + (1 - c_{\mathrm{hfx}})(ia\sigma|f_{\mathrm{xc}}|jb\sigma'), \end{aligned} \tag{4}$$

where c_{hfx} is the fraction of HFX and $f_{\mathrm{xc}}(\mathbf{r},\mathbf{r}')$ is the semilocal exchange–correlation kernel.[1] Only $\mathbf{A}$ (and not $\mathbf{B}$) is needed within the Tamm–Dancoff approximation (TDA), where one sets $\mathbf{y} = \mathbf{0}$ to obtain

$$\mathbf{A}\mathbf{x} = \omega\mathbf{x}. \tag{5}$$

B. Collinear SF-TDDFT

In SF-TDDFT, the excitation space is extended to include non-spin-conserving excitations of the form $\psi_{i\alpha} \to \psi_{a\beta}$. These allow access to spin-S target states starting from a spin-$(S+1)$ reference determinant. In this way, both ground and excited states of spin S are treated on the same theoretical footing, providing a balanced description of both.

When considering $\alpha \to \beta$ spin-flip excitations and assuming that the exchange–correlation kernel f_{xc} originates from a semilocal generalized gradient approximation (GGA), the coupling matrix elements simplify substantially. In this case, the Coulomb and semilocal parts vanish, and only the HFX term survives, since only HFX couples different spin components.[8] Consequently, the spin-flip coupling matrices take the form

$$A_{i\bar{a},j\bar{b}} = \delta_{ij}\delta_{\bar{a}\bar{b}}(\varepsilon_{\bar{a}} - \varepsilon_i) - c_{\mathrm{hfx}}(ij|f_{\mathrm{xc}}|\bar{a}\bar{b}), \tag{6a}$$

$$B_{i\bar{a},\bar{j}b} = -c_{\mathrm{hfx}}(ib|f_{\mathrm{xc}}|\bar{a}\bar{j}). \tag{6b}$$

(Bars on $\bar{a}$, $\bar{b}$, etc., indicate β-spin MOs.)

A variety of studies of this collinear formulation of SF-TDDFT have arrived at the conclusion that $c_{\mathrm{hfx}} \approx 0.5$ (i.e., 50% HFX) is optimal for both vertical excitation energies and singlet–triplet gaps.[8,35,58] In practice, the BH&HLYP functional,

$$E_{\mathrm{xc}}^{\mathrm{BH\&HLYP}} = \frac{1}{2}\left(E_{\mathrm{x}}^{\mathrm{B88}} + E_{\mathrm{x}}^{\mathrm{HFX}}\right) + E_{\mathrm{c}}^{\mathrm{LYP}}, \tag{7}$$

has become the standard choice for collinear SF-TDDFT calculations.[7] This is somewhat different from the "50/50" functional that is sometimes used for SF-TDDFT,[8,56] but BH&HLYP in Eq. (7) is the more common way to implement a functional with $c_{hfx} = 0.5$. A recent re-evaluation of BH&HLYP,[63] for both ground-state properties and (spin-conserving) LR-TDDFT excitation energies, concludes that this functional is superior in many ways to B3LYP (the latter with $c_{hfx} = 0.2$), except in the case of atomization energies.[63]

The excitation space generated by SF-TDDFT is depicted in Fig. 1 for a simple (4e, 4o) model with four electrons in four orbitals, wherein singlet excited states are generated from a high-spin triplet reference determinant. Excitations within the space of half-filled orbitals (labeled O → O in Fig. 1) generate a spin-complete manifold that includes one doubly excited determinant, which is the one that is needed to obtain proper topology at a S_0/S_1 conical intersection.[3–6] However, SF-TDDFT also generates additional determinants that are missing their spin complements, within the C → O, O → V, and C → V excitation spaces shown in Fig. 1. Any excited state that contains a significant contribution from a determinant in one of these subspaces will exhibit spin contamination.

C. MRSF-TDDFT

MRSF-TDDFT is based on a reference state whose density matrix is a linear combination of the $M_S = 1$ and $M_S = -1$ components of a triplet reference,[7,10,41]

$$\rho_0^{\mathrm{MR}}(\mathbf{r},\mathbf{r}') = \frac{1}{2}\left[\rho_0^{M_S=+1}(\mathbf{r},\mathbf{r}') + \rho_0^{M_S=-1}(\mathbf{r},\mathbf{r}')\right]. \tag{8}$$

The two components of this density matrix are subjected to separate spin-flipping operations: $\alpha \to \beta$ for the $M_S = 1$ component (as in conventional SF-TDDFT) and $\beta \to \alpha$ for the $M_S = -1$ component, as shown for a (4e, 4o) model in Fig. 2.

Comparing Figs. 1 and 2, it is evident that MRSF-TDDFT introduces many more electronic configurations compared to SF-TDDFT. Operationally, this removes the majority of the spin contamination even though the excitation space is not formally

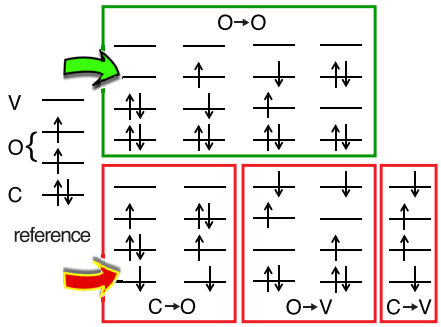

FIG. 1. Illustration of the SF-TDDFT excitation space for a (4e, 4o) model. Starting from a high-spin triplet reference determinant, single excitations combined with $\alpha \to \beta$ spin flip generate the determinants indicated in the O → O space (green box), which is a minimalist model for a S_0/S_1 conical intersection. However, determinants in the remaining three subspaces are each missing one or more spin complements that are needed to form $\hat{S}^2$ eigenstates. Adapted with permission from Zhang and Herbert, J. Chem. Phys. **143**, 234107 (2015). Copyright 2015 American Institute of Physics.

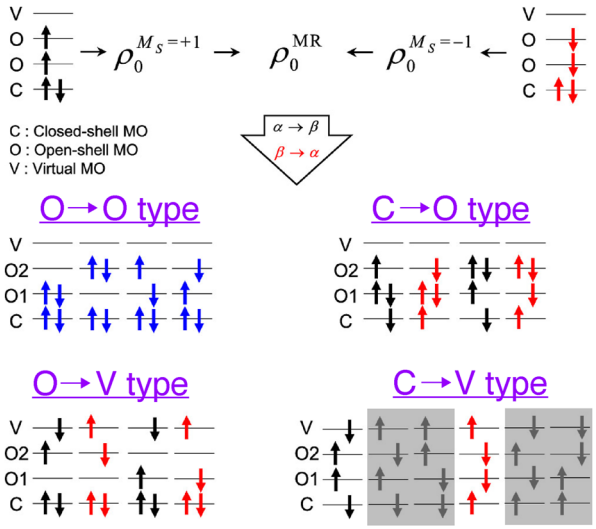

FIG. 2. Schematic illustration of MRSF-TDDFT for a (4e, 4o) model. An excitation space for singlet excited states is generated starting from both high- and low-spin triplet configurations, via single excitations combined with either $\alpha \to \beta$ spin flip (for $M_S = 1$) or $\beta \to \alpha$ spin flip (for $M_S = -1$). The four determinants shown in gray in the C → V subspace are missing from the excitation manifold because they cannot be generated in this manner. Adapted with permission from Horbatenko *et al.*, J. Chem. Theory Comput. **17**, 848–859 (2021). Copyright 2021 American Chemical Society.

spin-complete because some of the necessary C → V determinants (shown in gray in Fig. 2) cannot be generated in the manner described.[23,41] These are higher-energy configurations, however, and they play little role in low-lying excited states. In practice, $\langle \hat{S}^2 \rangle \approx 0$.[41]

MRSF-TDDFT is formulated only for singlet excited states. Its derivation is based on the density matrix formulation of the time-dependent KS methodology,[62] which means that the density matrix needs to be idempotent. This can be demonstrated for the density matrix in Eq. (8) based on a complex rotation of the spin functions.[41] Separation of the $M_S = 1$ and $M_S = -1$ triplet density matrices leads to a pair of TDA-like eigenvalue equations,

$$\mathbf{A}_s\mathbf{x}_s = \omega_s\mathbf{x}_s \tag{9a}$$

$$\mathbf{A}_t\mathbf{x}_t = \omega_t\mathbf{x}_t, \tag{9b}$$

for the singlet and triplet excited states, respectively. Coupling matrix elements between determinants from the $M_S = 1$ and $M_S = -1$ parts of the calculation are then added on an *ad hoc* basis.[41] This amounts to new contributions to the orbital Hessian,[41] of the form

$$A'_{pq,rs} = c_{\mathrm{hfx}}\left\langle \Phi^{M_S=+1}_{p\alpha q\beta} \middle| \hat{H} \middle| \Phi^{M_S=-1}_{r\beta s\alpha} \right\rangle. \tag{10}$$

The orbital Hessian that is used in practice is $\mathbf{A}_k + \mathbf{A}'$, for k = s or t in Eq. (9). As with SF-TDDFT, use of a functional with 50% HFX is found to be optimal[42] and BH&HLYP is again the standard choice.[7]

D. SA-SF-TDDFT

Collinear SF-TDDFT often suffers from significant spin contamination that is frequently worse than the corresponding (spin-conserving) LR-TDDFT calculation for the same system. This problem tends to grow worse as one moves away from the ground-state geometry on an excited-state potential surface, accessing bond-breaking geometries.[24] For excited-state geometry optimizations and molecular dynamics simulations, this necessitates use of a state-following procedure that attempts to follow a surface of consistent character.[18,24,64] State-following is not guaranteed to work.[15]

Operationally, spin contamination is largely eliminated by using the MRSF-TDDFT approach,[41] but an alternative is the SA-SF-TDDFT method.[24] This is a spin-complete extension of collinear SF-TDDFT that is rigorously free of spin contamination. Its formulation begins from SA-SF-CIS, which is based on a tensor equation-of-motion formalism.[30] Within this framework, the excited-state tensor $|xS_f\rangle\rangle$ is generated from a reference state $|S_0\rangle\rangle$ by the action of a rank-λ tensor operator, $\hat{O}^\dagger_{x\lambda}$:

$$\hat{O}^\dagger_{x\lambda}\left|S_0\right\rangle\rangle^{S_f} = |xS_f\rangle\rangle, \tag{11a}$$

$$\hat{O}_{x\lambda}|S_0\rangle\rangle = 0. \tag{11b}$$

Among the three equivalent tensor equations of motion that can be derived from Eq. (11), SA-SF-TDDFT uses

$$\begin{aligned}\sum_{ij\Gamma}(-1)^{S_0-S_f-\Gamma-\lambda_i}(2\Gamma+1)^{1/2}W(\lambda_i\lambda_j S_0 S_0;\Gamma S_f)\\ \times\left\langle S_0\middle\|\hat{\tilde{O}}_{y\lambda_i}\times[\hat{H},\hat{O}^\dagger_{x\lambda_j}]_\Gamma\middle\|S_0\right\rangle = \omega_{xS_f}\sum_{ij\Gamma}(-1)^{S_0-S_f-\Gamma-\lambda_i}\\ \times(2\Gamma+1)^{1/2}W(\lambda_i\lambda_j S_0 S_0;\Gamma S_f)\left\langle S_0\middle\|\hat{\tilde{O}}_{y\lambda_i}\times\hat{O}^\dagger_{x\lambda_j\Gamma}\middle\|S_0\right\rangle.\end{aligned} \tag{12}$$

This can be recast in matrix form as

$$\mathbf{Mz}(x) = \omega_x\mathbf{Nz}(x), \tag{13}$$

where $\mathbf{M}$ and $\mathbf{N}$ are matrices containing Hamiltonian commutators and overlap terms, respectively. The spin-flip excitation operators are expressed as triplet-coupled tensors,

$$\hat{O}^\dagger_{pq}(1,1) = -\hat{a}^\dagger_p\hat{a}_{\bar{q}}, \tag{14a}$$

$$\hat{O}^\dagger_{pq}(1,0) = \left(\hat{a}^\dagger_p\hat{a}_q - \hat{a}^\dagger_{\bar{p}}\hat{a}_{\bar{q}}\right)/\sqrt{2}, \tag{14b}$$

$$\hat{O}^\dagger_{pq}(1,-1) = \hat{a}^\dagger_{\bar{p}}\hat{a}_q, \tag{14c}$$

which ensures that only spin-pure configurations contribute. This construction removes the over-completeness of the excitation space and affords proper spin eigenstates while maintaining asymptotic scaling of $\mathcal{O}(N^4)$, the same as conventional TDDFT.

To incorporate dynamical correlation, SA-SF-TDDFT applies an empirical correction to the SA-SF-CIS matrix elements,[24] in the spirit of the DFT/MRCI method.[65] This correction replaces the Hamiltonian matrix elements by their KS analogs,[24]

$$\begin{aligned}\langle\Phi_{pq}|\hat{H}_{\mathrm{DFT}} - E_0^{\mathrm{DFT}}|\Phi_{rs}\rangle = \delta_{qs}F_{pr} - \delta_{pr}F_{qs} + \langle \mathrm{ps}\|qr\rangle\\ + (1-c_{\mathrm{hfx}})\langle \mathrm{ps}|rq\rangle.\end{aligned} \tag{15}$$

For the BH&HLYP functional, $1 - c_{\mathrm{hfx}} = 0.5$ and this affords the SA-SF-TDDFT model that includes dynamical correlation without spin contamination and provides correct topology at conical intersections.

E. Computational details

All TDDFT calculations were performed using Q-Chem v. 6.3,[66] with the exception of MRSF-TDDFT calculations that were performed using GAMESS [v. 15 July 2024 (R2) Patch 1].[67] Molecular geometries, obtained at the CC3/aug-cc-pVTZ level, were taken from the QUEST database.[45]

For LR-TDDFT calculations, we primarily employ the B3LYP functional as a representative choice because it remains a best performer,[1] with more modern functionals offering at best very slight statistical improvements ($\lesssim$0.1 eV).[1,68] However, we will also test ωB97M-V as a next-generation best-performer,[68] along with the BH&HLYP functional whose performance is comparable to B3LYP for many different properties.[63] BH&HLYP is also the standard choice for SF-, MRSF-, and SA-SF-TDDFT calculations[7] and is used for each of those methods. Unless otherwise specified, all calculations reported here use the aug-cc-pVTZ basis set, which is sufficient to obtain converged excitation energies using TDDFT.[1] TDDFT calculations use the SG-1 quadrature grid[69] except in the case of ωB97M-V, where SG-2 is used instead.[70]

All SA-SF-TDDFT calculations begin from a ground-state self-consistent field calculation performed using the "different orbitals for different spins" (DODS) variant of restricted open-shell (RO)KS.[71] This formulation satisfies both the Koopmans and Brillouin conditions and, in our experience, provides improved stability for non-*aufbau* solutions to the KS equation, ensuring the resulting MOs possess the correct spatial symmetry and spin character.[72] Therefore, we use the DODS orbitals as an initial guess to seed the SA-SF-TDDFT calculations. In a few cases, such as the H_2PO and F_2BO molecules from the QUEST 4 dataset,[73] failure to use DODS orbitals as a guess results in an incorrect ground-state KS solution and large errors in the excitation energies (e.g., ~2 eV for F_2BO).

III. RESULTS AND DISCUSSION

In the main part of this work, we compute excitation energies for various molecules in the QUEST database.[45] These results will be analyzed across different subsets of QUEST that span a range of systems sizes and also include datasets of CT transitions, doublet radicals, and doublet-to-quartet transitions. In addition, we consider excitation energies of small diradicals and inverted singlet–triplet gaps in nitrogen heterocycles.

In most cases, two or three low-lying excited states are considered for each molecule and we compare TDDFT/aug-cc-pVTZ excitation energies (ΔE) to reference values (ΔE_{ref}). Errors are defined as

$$\mathrm{error} = \Delta E - \Delta E_{\mathrm{ref}}, \tag{16}$$

so that positive errors imply overestimated excitation energies.

Most of the discussion that follows is divided along the lines of the various subsets of QUEST. Before embarking on that analysis, however, Fig. 3 summarizes the results across all of the QUEST datasets, illustrating the overall performance of several methods and providing comprehensive error statistics, including the mean absolute error (MAE) and the root-mean-square error (RMSE). Errors for various subsets of QUEST are tabulated below, and the accuracy for each subset can be compared to the aggregate assessment in Fig. 3. Overall, SA-SF-TDDFT exhibits both a smaller spread of errors as compared to conventional (spin-contaminated) SF-TDDFT and also shows no systematic error. SA-SF-TDDFT is also an improvement compared to TD-B3LYP, which we use as a baseline representing conventional LR-TDDFT.

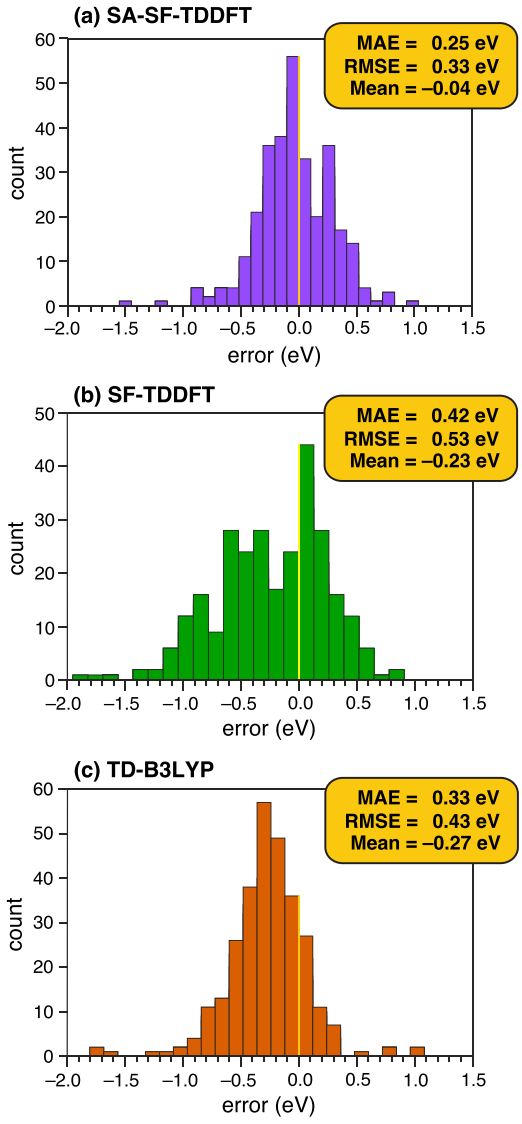

FIG. 3. Error distributions for vertical excitation energies computing using TDDFT/aug-cc-pVTZ, aggregated across all QUEST datasets and measured with respect to TBE reference values from Ref. 74 [Eq. (16)]. Both SA-SF-TDDFT and SF-TDDFT use the BH&HLYP functional.

A. QUEST 1: Small molecules

The QUEST 1 dataset consists of 18 small molecules ranging in size from one to three non-hydrogen atoms (Fig. 4).[75] Excitation energies computed for this dataset are presented in Table S1 and errors in SF-TDDFT, SA-SF-TDDFT, and TD-B3LYP calculations are summarized in Fig. 5. Figure 6 shows the correlation between TDDFT excitation energies and TBE values.

Transitions in the QUEST 1 dataset are singlets and triplets and for the former, the SF-TDDFT calculations employ a triplet reference state. The first computed singlet excitation energy thus corresponds to the singlet–triplet gap, which might be negative.

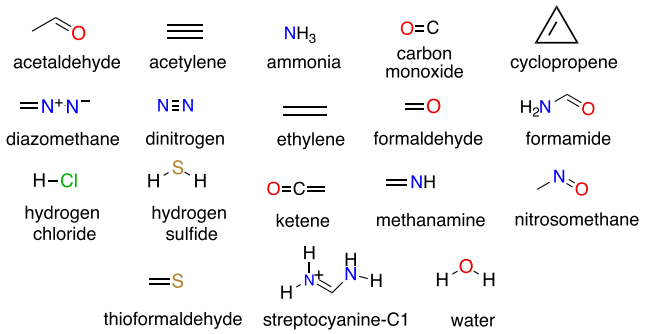

FIG. 4. QUEST 1 dataset of small molecules, assembled in Ref. 75. Streptocyanine-C1 is a cation.

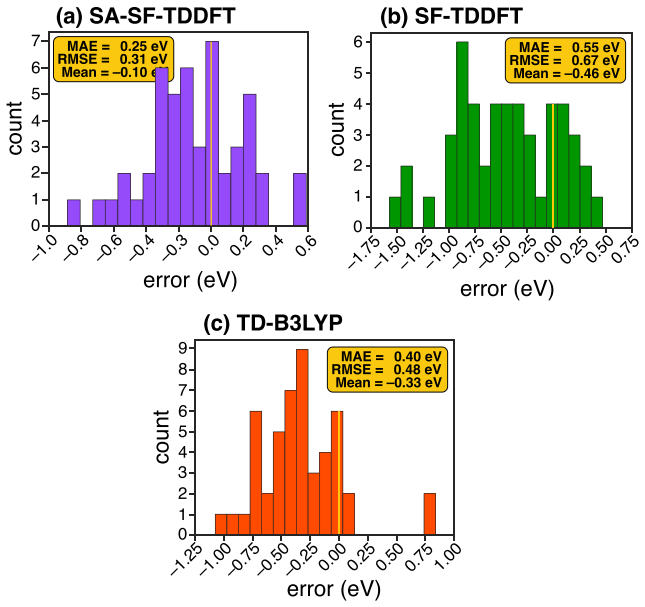

FIG. 5. Errors in TDDFT/aug-cc-pVTZ vertical excitation energies for the QUEST 1 dataset of small-molecule transitions, with respect to TBE values from Ref. 75. Numerical data are presented in Table S1.

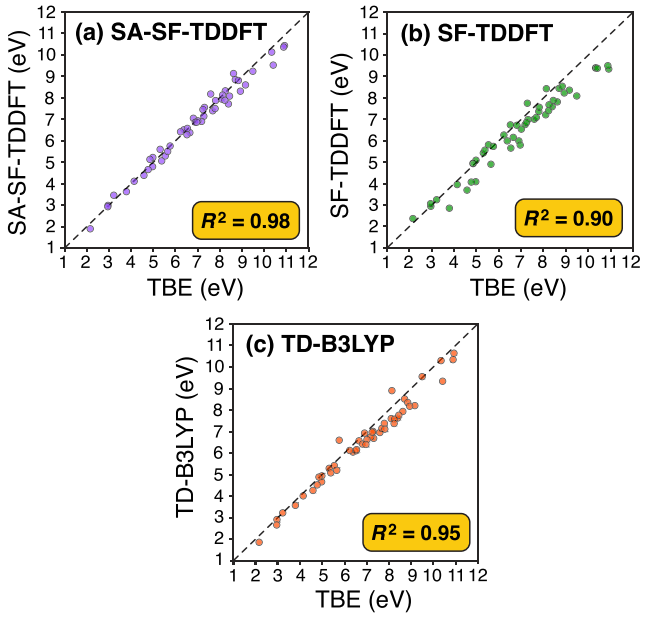

FIG. 6. Correlation between TDDFT/aug-cc-pVTZ excitation energies and TBE values[75] for the QUEST 1 dataset of small-molecule transitions. Numerical data are presented in Table S1.

In several cases, however, we observe that some of the computed excited states exhibit $\langle \hat{S}^2 \rangle > 2.0$, indicating significant spin contamination. For such instances, we identified those states as the true triplet states and accordingly evaluated the excitation energy as the energy difference between the singlet state and the corresponding triplet state.

Among the three TDDFT methods tested, SF-TDDFT (with the BH&HLYP functional) affords the largest deviation from the reference values, with a MAE of 0.55 eV. Comparison with SA-SF-TDDFT results using the same functional (MAE = 0.25 eV) suggests that the larger error in SF-TDDFT is a result of spin contamination. The accuracy of the spin-pure SA-SF-TDDFT method surpasses that of conventional TD-B3LYP, with MAE = 0.40 eV for the latter.

Notably, the water molecule is a challenge for all three methods and errors are relatively large for H_2O. Errors for the $^1B_1$ transition range from −0.5 eV (SA-SF-TDDFT) to +0.8 eV (SF-TDDFT), while those for the $^1A_2$ state are all in the range of 0.9–1.1 eV. It is unclear to us why this particular case is so challenging, but the problem persists with other density functionals. For example, ωB97M-V/aug-cc-pVTZ excitation energies exhibit errors of −0.76 eV for the $^1B_1$ transition, −1.05 eV for $^1A_2$, and −0.61 eV for $^3B_2$.

Another interesting case is the streptocyanine-C1 cation (Fig. 4). At the TD-B3LYP level, this molecule exhibits a pronounced blue shift in its $^1B_2$ excitation energy, with an error of 0.77 eV. Streptocyanine dyes are known to be problematic for standard hybrid functionals,[76–83] and even the modern ωB97M-V/aug-cc-pVTZ approach affords an error of 0.65 eV for the $^1B_2$ transition. Errors are smaller with SF methods, namely, 0.30 eV for SF-TDDFT and <0.01 eV for SA-SF-TDDFT. We will return to this in considering the QUEST 5 dataset (Sec. III C), which contains two streptocyanine examples.

B. QUEST 3: Medium-sized molecules

QUEST 3 is by far the largest of the QUEST datasets, comprising highly accurate vertical transition energies for 27 closed-shell organic molecules containing 4–6 non-hydrogen atoms, including several aromatic compounds (Fig. 7).[84] Full TDDFT results for QUEST 3 are provided in Tables S2 and S3. Errors are summarized in Fig. 8, and correlations with TBE values can be found in Fig. 9.

For QUEST 3, we observe trends that are similar to those seen for QUEST 1. In particular, SA-SF-TDDFT provides the most accurate results, followed by TD-B3LYP and then SF-TDDFT. Previous studies report that collinear SF-TDDFT performs poorly for singlet–triplet vertical gaps, and our results confirm this behavior. Errors exceed 0.8 eV for singlet–triplet gaps in acetone, acrolein,m cyanoformaldehyde, cyclopropenone, and propynal (see Table S2). Furthermore, the correlation between SF-TDDFT transition energies and TBE values is the weakest among the methods tested, with $R^2 = 0.85$ vs $R^2 = 0.94$ for SA-SF-TDDFT (Fig. 9).

For this dataset, we also tested MRSF-TDDFT. We find that this approach, which is based here on the BH&HLYP functional, closely tracks the TD-B3LYP results and affords a MAE of 0.35 eV that is scarcely distinguishable from TD-B3LYP (Fig. 8). This does represent an improvement over SF-TDDFT, whose MAE is 0.42 eV for the same dataset. Nevertheless, SA-SF-TDDFT delivers consistently smaller deviations from the reference values.

C. QUEST 5: Intermediate-size molecules

The relatively new QUEST 5 dataset includes 13 additional systems, ranging from small to moderately large molecules (Fig. 10).[45] The results from all methods, summarized in Figs. 11 and 12 and provided in detail in Table S6, are consistent with results from the datasets considered above. In particular, MAEs for QUEST 5 are 0.26 eV for SA-SF-TDDFT, 0.40 eV for SF-TDDFT, and 0.35 eV for TD-B3LYP.

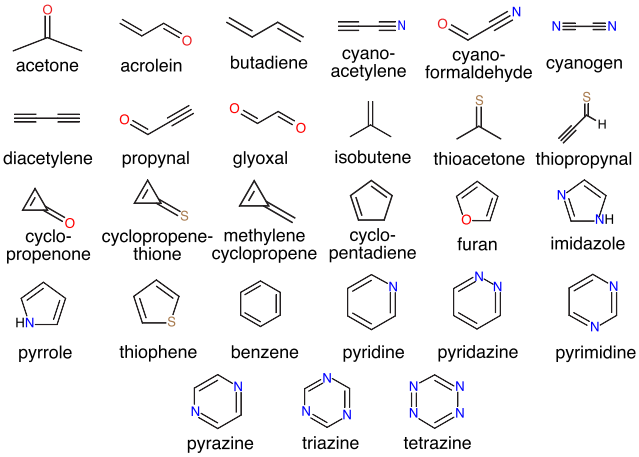

FIG. 7. QUEST 3 molecular dataset, assembled in Ref. 84.

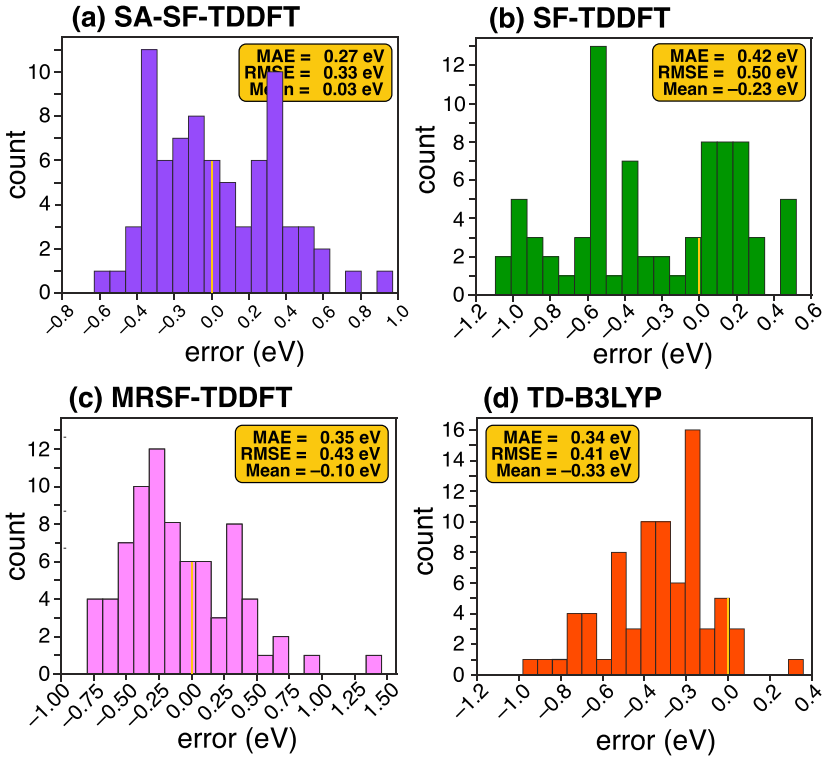

FIG. 8. Errors in TDDFT/aug-cc-pVTZ vertical excitation energies (with respect to TBE values from Ref. 84) for the QUEST 3 dataset of transition energies in medium-size molecules. Numerical data are presented in Tables S2 and S3.

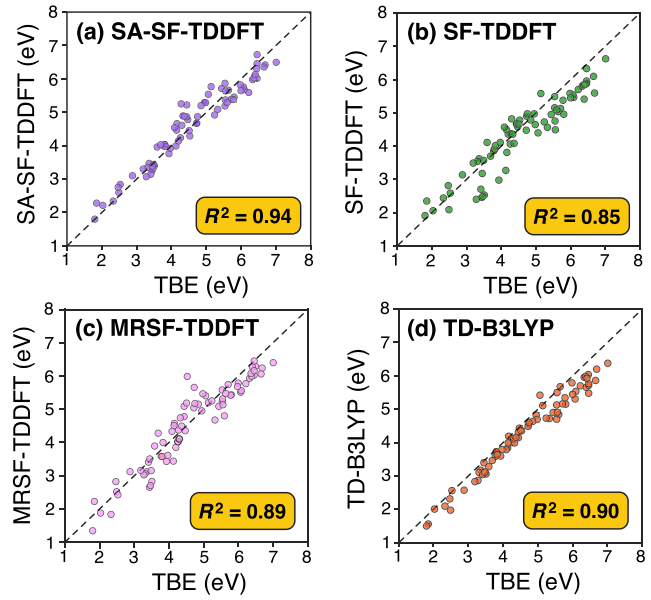

FIG. 9. Correlation between TDDFT/aug-cc-pVTZ excitation energies and TBE values,[84] for the QUEST 3 dataset of medium-sized molecules. Numerical data are presented in Tables S2 and S3.

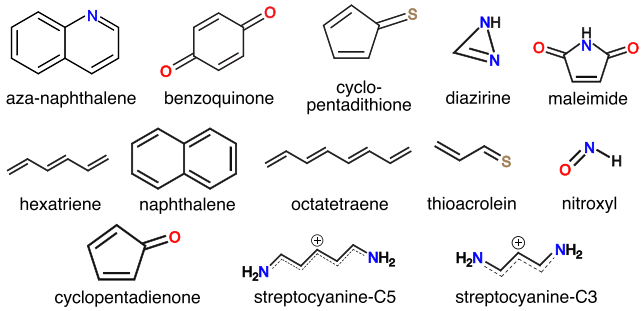

FIG. 10. QUEST 5 molecular dataset, assembled in Ref. 45. The two streptocyanines are cations.

QUEST 5 contains two cationic streptocyanine dyes, a different example of which proved problematic for TD-B3LYP in Sec. III A. These species, which are also known as linear cyanines, are challenging cases that are known to be problematic for standard hybrid functionals such as B3LYP and PBE0.[76–83] Some double hybrid functionals perform better,[85,86] as do some meta-GGA functionals.[87] For these particular dyes, at least part of the issue with discrepancies between TDDFT calculations and experiment lies in pronounced non-vertical character in their transitions,[88] which

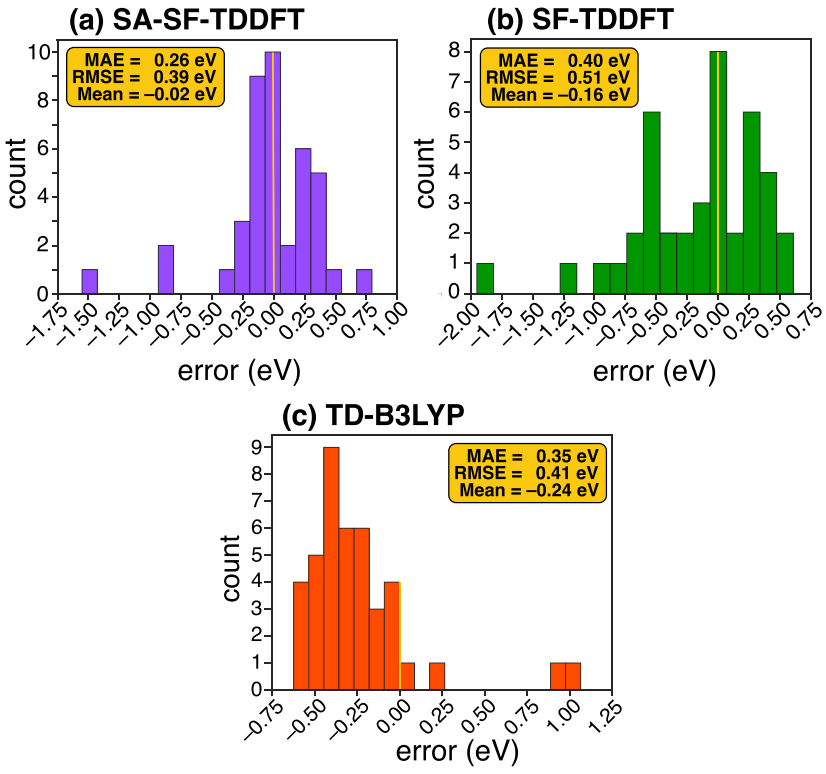

FIG. 11. Errors in TDDFT/aug-cc-pVTZ vertical excitation energies (with respect to TBE values from Ref. 45) for the QUEST 5 dataset. Numerical data are presented in Table S6.

complicates direct comparison with experiment. Another part of the issue is a relatively large density change upon $S_0 \rightarrow S_1$ excitation,[78] which may be better described by double hybrid functionals.

Our results confirm that TD-B3LYP is significantly less accurate as compared to the same functional applied to the other molecules in QUEST 5. Considering the $^1B_2(\pi \rightarrow \pi^*)$ transition and including the streptocyanine-C1 molecule from the QUEST 1 dataset, the TD-B3LYP errors are 0.77 eV (for C1), 0.97 eV (for C3), and 1.06 eV (for C5). This is not simply a B3LYP artifact, as errors are also large at the ωB97M-V/aug-cc-pVTZ level: 0.65 eV (C1), 0.74 eV (C3), and 0.75 eV (C5). However, both SF- and SA-SF-TDDFT provide much better accuracy in all three cyanine molecules. For the $^1B_2$ transition, the errors are 0.3–0.4 eV when using SF-TDDFT, while for SA-SF-TDDFT the errors range from zero to −0.1 eV. Elsewhere, SF-TDDFT has been shown to improve the accuracy of transition energies for boron-dipyrromethene difluoride (BODIPY) dyes,[89] which are subject to some of the same challenges as cyanine dyes.[90–94]

D. QUEST 6: CT excitations

The QUEST 6 dataset contains 17 molecules exhibiting intramolecular CT excitations (Fig. 13).[95] The performance of TD-B3LYP is known to be poor for such transitions,[1] but we include it in our comparison in order to set a baseline. For a more robust description of CT transitions, we turn to conventional LR-TDDFT using the long-range corrected[96–98] (LRC) functional LRC-ωPBE,[99,100] adjusting the range-separation parameter (ω) for each separate system using the global density-dependent (GDD) tuning scheme.[101,102] We refer to this functional as LRC-ω_{GDD}PBE to indicate the tuning, and tuned values ω_{GDD} can be found in Table S7. Details of the GDD procedure can be found elsewhere,[102] along with a broader assessment of the LRC-ω_{GDD}PBE functional in LR-TDDFT calculation.

Errors for the QUEST 6 dataset are summarized in Fig. 14 and numerical data are provided in Table S8. For SF-TDDFT, we encountered numerous cases where it was difficult to unambiguously identify the appropriate CT state based on symmetry considerations. As such, SF-TDDFT is excluded from this analysis.

Correlations between TBE and TDDFT values are shown in Fig. 15. As expected, TD-B3LYP affords larger errors than seen above, with a MAE value of 0.55 eV and a relatively poor correlation coefficient ($R^2 = 0.7$). Moreover, it is clear that transition energies are mostly underestimated by TD-B3LYP calculations, sometimes substantially. In comparison, SA-SF-TDDFT exhibits a MAE of 0.22 eV with a correlation coefficient $R^2 = 0.96$. An important distinction is that SA-SF-TDDFT employs the BH&HLYP functional, with $c_{hfx} = 0.5$ as compared to $c_{hfx} = 0.2$ for B3LYP. Even within the context of conventional LR-TDDFT, the BH&HLYP functional corrects the underestimation of CT energies for medium-sized organic molecules and actually pushes the errors slightly in the opposite direction, toward overestimation.[63] This does not seem to be the case for SA-SF-TDDFT based on the same functional.

Notably, the SA-SF-TDDFT error for this CT dataset is only slightly larger than the MAE of 0.16 eV that we obtain using TD-LRC-ω_{GDD}PBE, the latter of which is a state-of-the-art approach for CT transitions. Thus, we conclude that SA-SF-TDDFT can safely

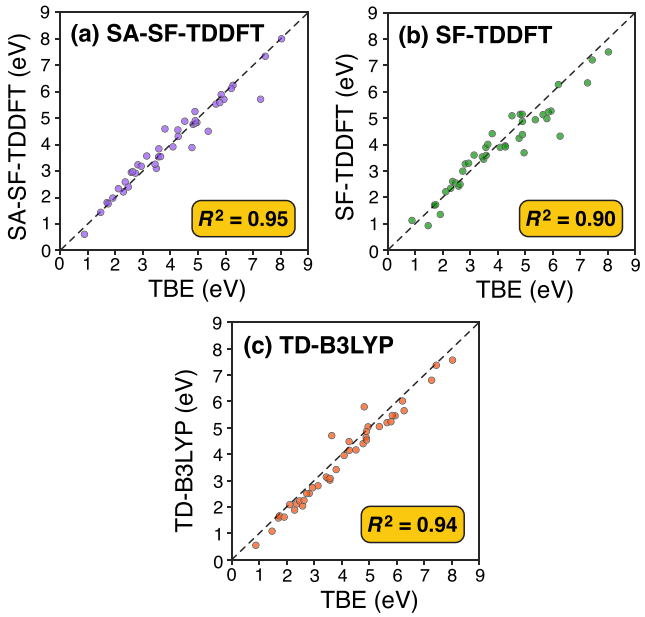

FIG. 12. Correlation between TDDFT/aug-cc-pVTZ excitation energies and TBE values[45] for the QUEST 5 dataset. Numerical data are presented in Table S6.

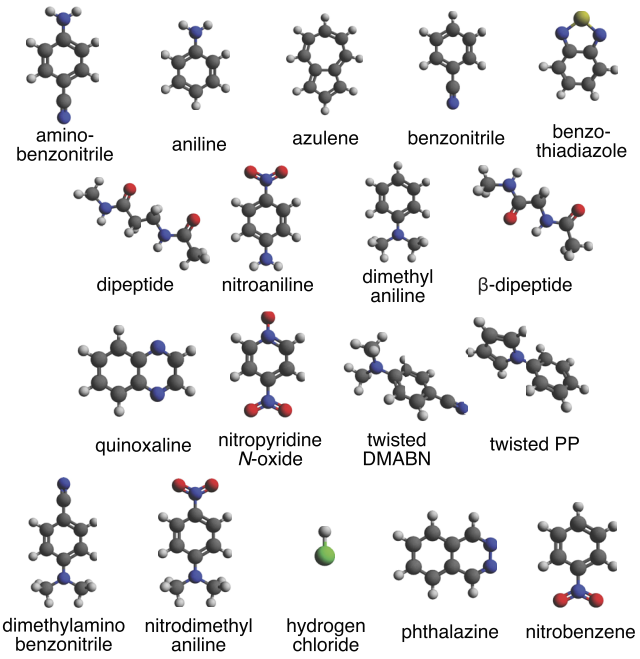

FIG. 13. QUEST 6 molecular dataset.

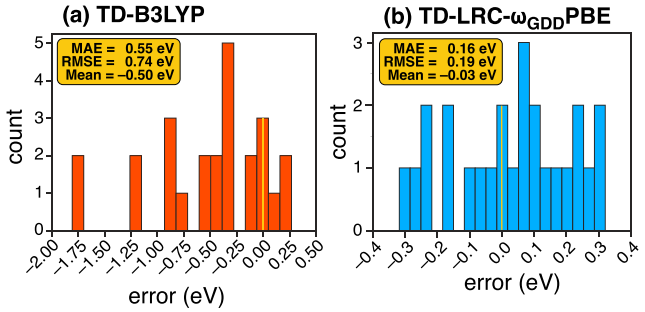

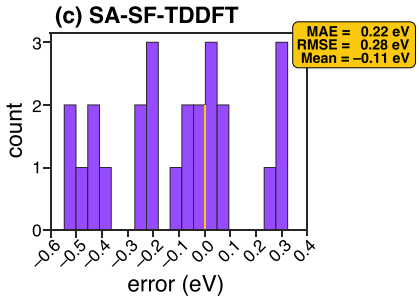

FIG. 14. Errors in TDDFT/aug-cc-pVTZ vertical excitation energies (with respect to TBE values from Ref. 95) for ^{1}CT transitions in the QUEST 6 dataset. Numerical data are provided in Table S8.

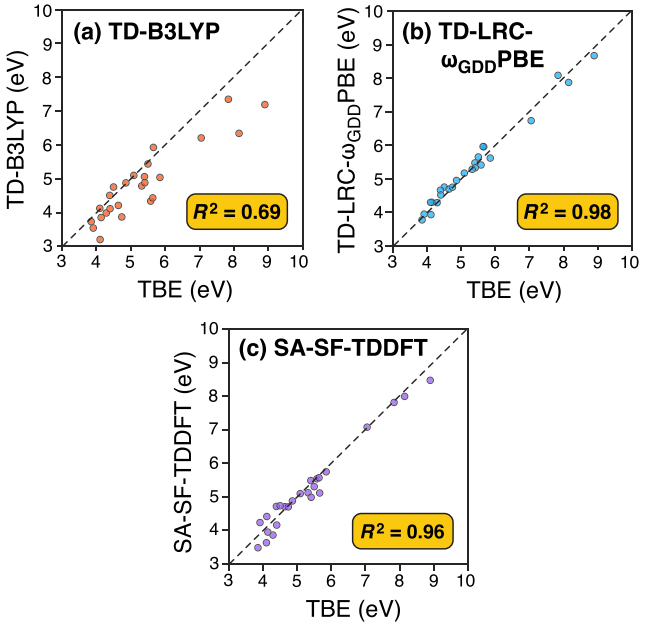

FIG. 15. Correlation between TDDFT/aug-cc-pVTZ excitation energies and TBE values,[95] for the QUEST 6 dataset of ^{1}CT transitions. Numerical data are provided in Table S8.

be used to describe intramolecular CT in medium-sized molecules. However, because its exchange–correlation potential decays as c_{hfx}/R,[1,103] the accuracy of this approach must eventually degrade for genuinely long-range CT because the electron–hole attraction is too weak as $R \to \infty$, for any functional with $c_{hfx} < 1$.[1,96]

E. QUEST 7: Bicyclic molecules

The QUEST 7 dataset includes the ten bicyclic molecules that are depicted in Fig. 16.[104] Errors are summarized in Fig. 17, and correlations between TDDFT and TBE transition energies

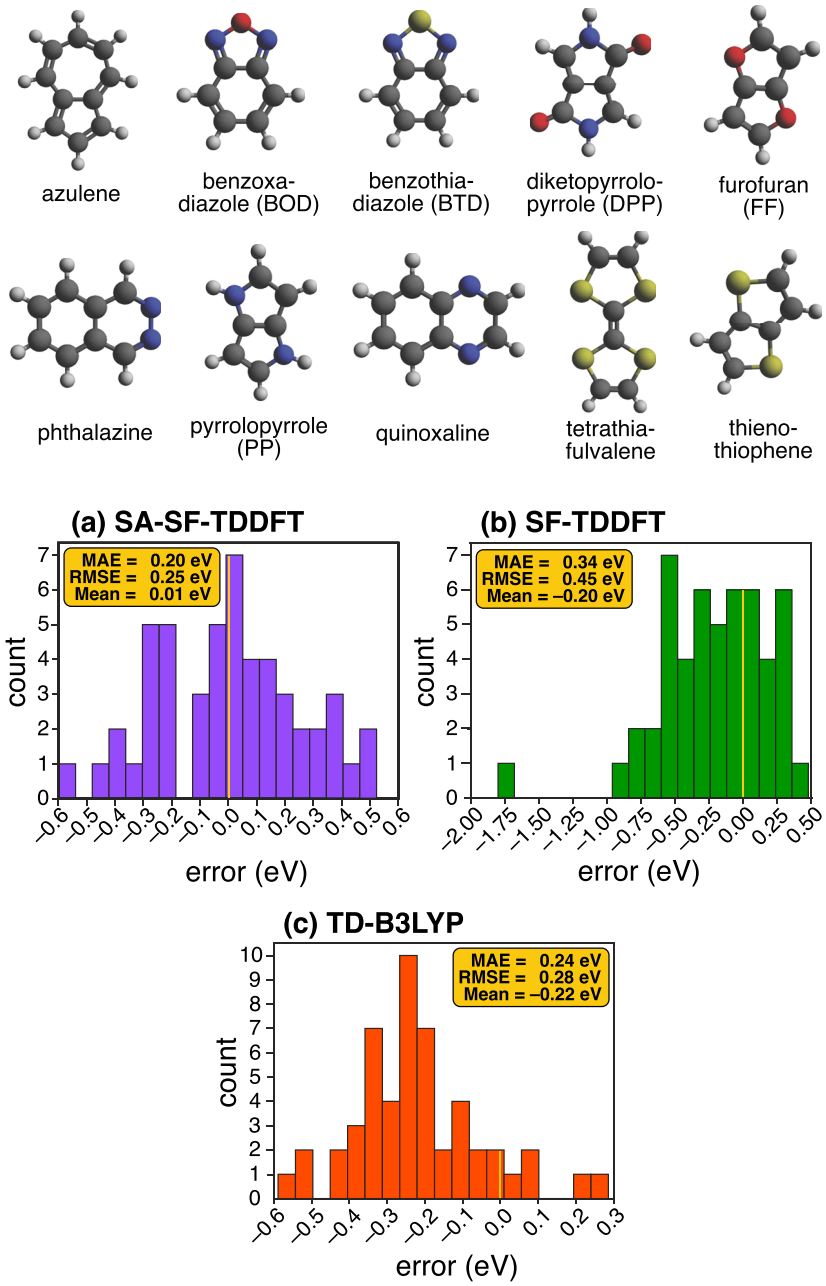

FIG. 16. QUEST 7 molecular dataset.

FIG. 17. Errors in TDDFT/aug-cc-pVTZ vertical excitation energies (with respect to TBE values from Ref. 104), for the QUEST 7 dataset of transitions in bicyclic molecules. Numerical data are provided in Table S9.

are shown in Fig. 18. Complete numerical data are provided in Table S9.

Interestingly, all methods tested here perform well for this set, including TD-B3LYP and both SF-TDDFT approaches. All three methods afford consistently accurate vertical excitation energies across all systems. The good performance can be attributed to the fact that bicyclic compounds generally possess rigid, well-defined molecular frameworks whose structural rigidity suppresses low-frequency vibrational distortions and minimizes geometry-induced orbital reordering. Thus, the character of the frontier MOs is preserved across different electronic structure methods and this improves the reliability of single-reference methods such as conventional TDDFT.

Moreover, extended π-conjugation in these bicyclic aromatic systems leads to transitions of the predominantly $\pi \rightarrow \pi^*$ character, with large spatial overlap between the excited electron and the hole.[105] This makes for compact transition densities that avoid long-range CT issues that are otherwise associated with TD-B3LYP calculations.[1,106,107] In the few cases where larger deviations are observed using TD-B3LYP, the errors

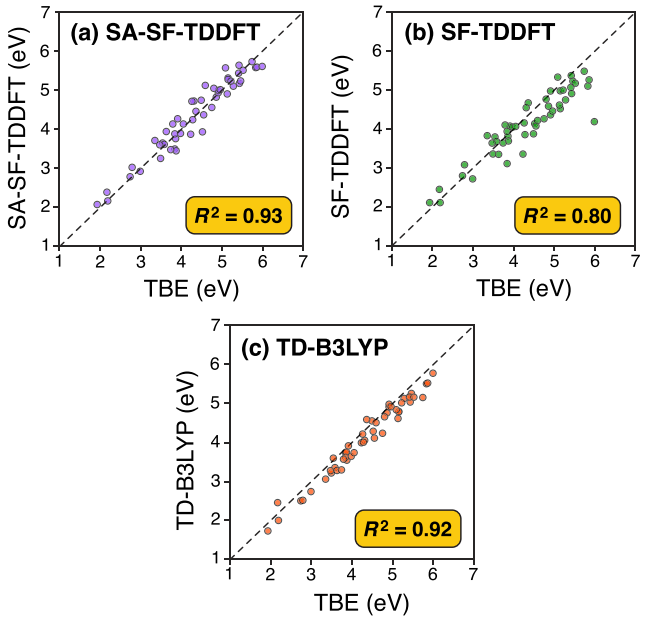

FIG. 18. Correlation between TDDFT/aug-cc-pVTZ excitation energies and TBE values,[104] for the QUEST 7 dataset of transitions in bicyclic molecules. Numerical data are provided in Table S9.

arise primarily from $n \rightarrow \pi^*$ excitations with partial CT character (see Table S9).

The delocalized π-systems of bicyclic molecules also exhibit relatively little static correlation, so that their low-lying excited states are adequately described by single-reference methods such as TD-B3LYP. (The azulene molecule does exhibit some multireference character in its S_2 state,[108] nevertheless TD-B3LYP errors are no larger than 0.3 eV.) As such, TD-B3LYP and SA-SF-TDDFT afford similar statistical performance for this dataset, with MAEs of 0.24 and 0.20 eV, respectively.

F. QUEST 4: Exotic and open-shell species

QUEST 4 consists of two subsets.[73] The first of these contains closed-shell molecules that are labeled as "exotic" because they contain at least one of the elements F, Cl, P, or Si. In particular, the molecules in this subset are carbonyl fluoride (CF_2O), CCl_2, CClF, CF_2, difluorodiazirine (CF_2N_2), formyl fluoride (CHFO), HCCl, HCF, HCP, HPO, HPS, HSiF, $SiCl_2$, and silylidene (CH_2Si). The second subset of QUEST 4 consists of open-shell species including allyl (C_3H_5), BeF, BeH, BH_2, CH, CH_3, CN, CNO, CON, CO^+, F_2BO, H_2BO, HCO, HOC, H_2PO, H_2PS, NCO, NH_2, nitromethyl (CH_2NO_2), NO, OH, and PH_2. These two subsets are considered separately in the discussion below.

1. Exotic species

For the "exotic" subset of QUEST 4, we computed excitation energies using both SF-TDDFT and SA-SF-TDDFT, along with TD-B3LYP to provide a baseline. Complete results are listed in Table S4, and the errors are listed in Table I. The spin-pure SA-SF-TDDFT method exhibits a MAE of 0.17 eV, which is much smaller than that of the spin-contaminated SF-TDDFT approach (MAE = 0.35 eV). TD-B3LYP also performs quite well, with a MAE of 0.16 eV. A similar trend is observed for the vertical singlet–triplet gaps, for which SF-TDDFT exhibits significantly larger errors relative to the spin-adapted formulation.

TABLE I. Performance of TDDFT methods for vertical transition energies of exotic molecules in the QUEST 4 dataset.

			Error (eV)[b]		
			Spin-flip[c]		
Molecule	State	TBE (eV)[a]	SF	SA-SF	TD-B3LYP
CF_2O	$^1A_2$	7.31	−0.34	0.43	−0.22
CF_2O	$^3A_2$	7.06	−1.15	−0.29	−0.50
CCl_2	$^1B_1$	2.59	0.05	−0.10	0.03
CCl_2	$^1A_2$	4.40	−1.02	−0.14	−0.24
CCl_2	$^3B_1$	1.22	0.44	−0.07	−0.10
CClF	$^1A''$	3.55	0.03	−0.17	0.04
CF_2	$^1B_1$	5.09	−0.12	−0.31	0.02
CF_2	$^3B_1$	2.77	0.59	−0.15	−0.25
CF_2N_2	$^1B_1$	3.74	−0.05	−0.11	−0.25
CF_2N_2	$^3B_1$	3.03	0.11	−0.28	−0.44
CHFO	$^1A''$	5.96	−0.43	0.35	−0.05
CHFO	$^3A''$	5.73	−1.12	−0.33	−0.46
HCCl	$^1A''$	1.98	0.12	−0.02	−0.03
HCF	$^1A''$	2.49	0.13	−0.02	−0.02
HCP	$^1\Sigma^-$	4.84	−0.85	−0.11	−0.17
HCP	$^1\Delta$	5.15	−0.47	−0.31	−0.48
HPO	$^1A''$	2.47	0.10	0.00	−0.03
HPS	$^1A''$	1.59	0.01	0.11	−0.02
HSiF	$^1A''$	3.05	0.25	−0.04	0.03
$SiCl_2$	$^1B_1$	3.91	0.12	−0.17	0.06
$SiCl_2$	$^3B_1$	2.48	0.38	0.12	−0.07
CH_2Si	$^1A_2$	2.11	0.03	−0.17	0.07
CH_2Si	$^1B_2$	3.78	−0.14	−0.03	0.15
MAE			0.35	0.17	0.16

[a] From Ref. 73.
[b] Relative to TBE values [Eq. (16)]. Calculations employ the aug-cc-pVTZ basis set.
[c] BH&HLYP functional.

2. Doublet radicals

Vertical excitation energies for the radical subset of QUEST 4 are compiled in Table S5, and errors for various theoretical methods are listed in Table II. (Five problematic systems in QUEST 4 have been removed from these tables and are considered separately, in Sec. III F 3.) Each of the QUEST 4 radicals has a doublet ground state, yet we observe an interesting trend in which SF- and SA-SF-TDDFT exhibit comparable performance, with MAEs of 0.38 and 0.31 eV, respectively. As indicated in Table II, this is not any better than conventional LR-TDDFT in a spin-unrestricted formalism. The functionals B3LYP, BH&HLYP, and ωB97M-V all exhibit MAEs of 0.3 eV for this dataset.

TABLE II. Performance of TDDFT methods for vertical transition energies of doublet radicals in the QUEST 4 dataset.[a]

			Error (eV)[c]				
			LR-TDDFT			Spin-flip[d]	
Molecule	State	TBE (eV)[b]	B3LYP	BH&HLYP	ωB97M-V	SA-SF	SF
Allyl	$^2B_1$	3.43	0.51	0.91	0.45	0.11	0.10
BeF	$^2\Pi$	4.15	0.01	0.05	−0.14	−0.61	−0.52
BeH	$^2\Pi$	2.49	0.09	0.12	−0.30	−0.20	−0.26
BeH	$^2\Pi$	6.45	−1.59	−1.28	−1.81	−0.20	−0.37
BH_2	$^2B_1$	1.18	0.16	0.16	−0.24	−0.10	0.00
CH	$^2\Delta$	2.94	0.29	0.29	0.14	0.07	−1.21
CH	$^2\Sigma^-$	3.31	0.23	−0.08	−0.09	−0.01	−0.26
CH_3	$^2A_1'$	5.86	−0.65	−0.12	−0.78	0.27	0.28
CH_3	$^2E'$	6.96	−0.74	−0.11	−0.80	0.09	0.19
CN	$^2\Pi$	1.38	−0.17	−0.17	−0.46	−0.82	−0.57
CO^+	$^2\Pi$	3.26	0.12	0.60	−0.00	−0.80	−0.60
F_2BO	$^2B_1$	0.71	−0.30	0.20	0.20	0.00	−0.05
F_2BS	$^2B_1$	0.48	−0.16	0.13	−0.14	0.00	0.00
H_2BO	$^2B_1$	2.17	−0.25	−0.01	0.08	−1.20	−1.15
HCO	$^2A''$	2.09	−0.17	0.31	0.08	0.30	0.19
HCO	$^2A'$	5.45	0.42	0.37	−0.55	0.75	0.61
HOC	$^2A''$	0.93	0.18	0.13	−0.12	−0.08	−0.11
H_2PO	$^2A''$	2.81	−0.10	0.08	−0.14	−0.67	−0.89
H_2PO	$^2A'$	4.21	0.15	0.03	0.07	0.42	0.63
H_2PS	$^2A''$	1.15	0.08	0.10	−0.15	−0.31	−0.34
NH_2	$^2A_1$	2.12	0.24	0.22	0.04	−0.02	0.06
CH_2NO_2	$^2B_2$	2.05	−0.10	0.53	0.28	−0.01	−0.29
PH_2	$^2A_1$	2.77	0.16	0.21	−0.14	−0.06	0.08
vinyl	$^2A''$	3.31	−0.01	0.13	−0.17	−0.35	−0.35
vinyl	$^2A'$	4.69	−0.18	0.14	−0.37	−0.44	−0.38
MAE (doublet transitions)			0.28	0.27	0.31	0.31	0.38
MAE (including quartets)[e]			...	...	...	0.31	0.41

[a]Five of the QUEST 4 species have been removed and are considered separately in Table IV.
[b]From Ref. 73.
[c]Relative to TBE values [Eq. (16)]. Calculations employ the aug-cc-pVTZ basis set.
[d]BH&HLYP functional.
[e]Including the doublet-to-quartet transitions from Table II.

Quartet excited states for doublet radicals were recently added to the QUEST database.[74] Error statistics for these doublet-to-quartet transitions are provided in Table III for two spin-flip methods. For TD-B3LYP, we did not find any excited states with $\langle \hat{S}^2 \rangle$ values in the range of 3.00–3.75 that might reliably be called quartet states, so LR-TDDFT results are excluded from Table III. Recently, a new spin-adapted "spin-flip-down" method called XSF-TDA has been reported and applied to these same doublet-to-quartet transitions.[29] That approach affords a MAE of 0.34 eV for this dataset, compared to the MAE of 0.31 eV for SA-SF-TDDFT.

3. Problematic linear doublets

For a doublet ground state, both SF- and SA-SF-TDDFT employ a high-spin quartet reference state. In cases where two of the three singly occupied MOs (SOMOs) are (near-)degenerate, whether by symmetry or by accident, the resulting excited states become artificially (near-)degenerate. This leads to physically incorrect state ordering and inaccurate excitation energies, a phenomenon that was noted recently by others.[109] This degeneracy issue makes high-symmetry doublet radicals intrinsically more challenging for both SF and SA-SF-TDDFT.

TABLE III. Performance of spin-flip methods for doublet-to-quartet transitions in the QUEST dataset.

			Error (eV)[b]	
Molecule	State	TBE (eV)[a]	SA-SF	SF
Allyl	$^4A_2$	6.01	−0.28	−0.54
BeH	$^4\Pi$	5.88	0.02	−0.26
BH_2	$^4A_2$	5.36	0.43	0.28
CH	$^4\Sigma^-$	0.72	0.31	0.23
CN	$^4\Sigma^+$	6.04	0.85	0.58
CO^+	$^4\Sigma^+$	7.28	−0.55	0.33
HCO	$^4A''$	6.39	−0.26	−0.67
H_2PO	$^4A''$	6.32	−0.49	−0.89
H_2PS	$^4A''$	5.12	−0.19	−0.41
NH_2	$^4B_1$	7.29	0.30	0.00
CH_2NO_2	$^4A_2$	4.34	−0.21	−0.86
PH_2	$^4A_2$	6.16	−0.10	0.93
vinyl	$^4A'$	4.56	−0.28	−0.50
MAE			0.33	0.50

[a]From Ref. 74.
[b]Relative to TBE values [Eq. (16)]. Calculations employ the aug-cc-pVTZ basis set and the BH&HLYP functional.

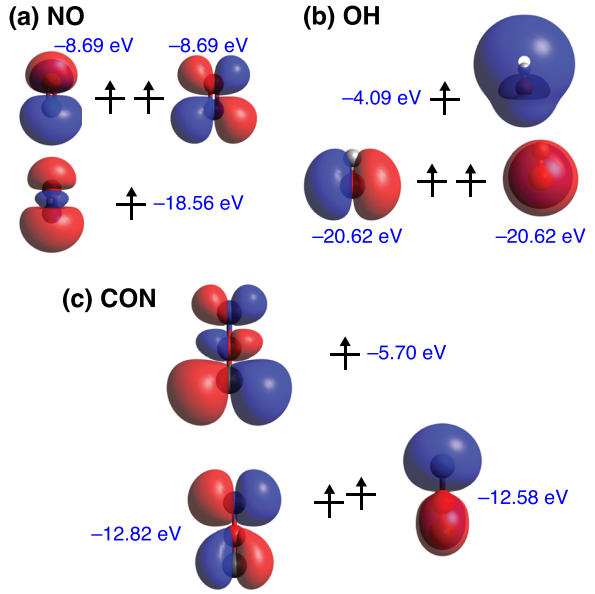

FIG. 19. Degenerate or near-degenerate SOMOs for quartet states of the (a) NO, (b) OH, and (c) CON radicals. In each case, a single excitation coupled to $\alpha \rightarrow \beta$ spin flip creates two (quasi-)degenerate determinants.

Diradicals with linear geometries (including diatomics) exhibit a symmetry-required degeneracy of the p_x and p_y orbitals, as shown for several examples in Fig. 19, and this is especially problematic. Five of the QUEST 4 radicals fall into this category: OH, NO, CNO, CON, and NCO. These species have degenerate SOMOs in the quartet reference (see Fig. 19), such that the high-spin quartet state creates a worse static correlation problem as compared to the doublet it replaces, because there are two low-lying degenerate or quasi-degenerate excitations out of the quartet SOMOs. This leads to erroneous excitation energies for SF-TDDFT methods.

The aforementioned systems have been segregated from Table S5 and relegated to Table IV, where we also present results from the "extended" (X)CIS approach.[72,110] The latter method was designed for doublet radicals and performs remarkably well for the five linear radicals that are problematic for SF methods. XCIS excitation energies are mostly good approximations to TBE values with two notable exceptions, OH($^2\Sigma^-$) and CON($^2\Sigma$), for which the XCIS errors are 1.0 and 0.9 eV, respectively. It is possible that a XCIS method with KS orbitals might reduce these errors by incorporating dynamical electron correlation, à la the DFT/CIS method,[31–33] and we are presently investigating this possibility.

We also tried to examine transition-metal complexes, which are difficult to describe because their ground states often contain degenerate SOMOs. However, the high-spin reference used in SF and SASF amplifies the problem encountered in using a quartet reference state for doublet radicals, as it creates degenerate SOMOs that lead to incorrect state ordering and unreliable excitation energies. A similar limitation was demonstrated long ago by Seth and Ziegler,[111] who showed that the use of non-degenerate TDDFT excitations provided an effective way to avoid this failure. Inspired by this approach, we plan to develop a similar strategy to construct non-degenerate high-spin reference states via artificial symmetry breaking, enabling a more robust description of open-shell transition metals.

TABLE IV. Vertical excitation energies for the problematic doublet radicals in QUEST 4.

		Excitation energy (eV)[a]			
Molecule	State	SF[b]	SA-SF[b]	XCIS	TBE
OH	$^2\Sigma^+$	7.76	8.66	4.02	4.10
OH	$^2\Sigma^-$	10.42	10.52	9.06	8.02
NO	$^2\Sigma^+$	7.00	8.15	6.30	6.13
NO	$^2\Sigma^+$	8.20	8.62	7.17	7.29
CNO	$^2\Sigma^+$	0.04	0.06	2.32	1.61
CNO	$^2\Pi$	5.87	6.26	5.17	5.49
CON	$^2\Pi$	0.08	0.28	3.67	3.53
CON	$^2\Sigma$	2.93	3.44	4.73	3.86
NCO	$^2\Sigma^+$	7.19	0.31	2.92	2.89
NCO	$^2\Pi$	8.07	7.62	4.26	4.73
MAE		2.18	2.19	0.40	⋯

[a]TDDFT and XCIS calculations use the aug-cc-pVTZ basis set and TBE values are from Ref. 73.
[b]BH&HLYP functional.

In principle, non-collinear SF-TDDFT can alleviate some of the artificial degeneracies that arise in the collinear formulation by allowing explicit mixing of spin components. This improves the description of certain open-shell systems.[61] In practice, however, non-collinear implementations often exhibit unphysical behavior, including numerical instabilities and large errors in excitation

energies, due to formal deficiencies in the treatment of transverse spin gradients in the exchange–correlation kernel.[59,112] These issues have been traced to the mathematical structure of non-collinear functionals beyond the local density approximation, where the exchange–correlation kernel involves spin-density terms that become ill-defined in regions of rapidly varying spin polarization.[9] Although there has been recent progress on resolving the numerical instabilities associated with non-collinear SF-TDDFT,[48,61] benchmark studies demonstrate that it sometimes artificially stabilizes mixed-spin states.[56] In such cases, the non-collinear variant performs worse, at least with GGAs, and comparable accuracy is achieved only in the presence of a substantial fraction of exact exchange.[56] Given these operational instabilities and the added complexity of non-collinear response kernels, the collinear SF-TDDFT formulation offers a more reliable and practical approach, especially when used with a hybrid functional such as BH&HLYP.

G. Diradicals

Diradicals are a distinctive class of molecules characterized by two unpaired electrons occupying nearly degenerate orbitals, leading to strong static correlation, unusual bonding patterns, and small singlet–triplet gaps. Their electronic structure cannot be described by a single dominant configuration, so traditional single-reference methods often fail to describe the energetics and state-ordering of diradicals. The original implementation of SF-TDDFT was specifically developed for the treatment of diradicals,[8] as their multi-configurational nature demands an approach that can handle near-degeneracies. By starting from a weakly correlated, high-spin reference and generating low-spin states through a single spin flip, SF-TDDFT naturally captures the essential correlated character of diradicals and provides a balanced and efficient description of their ground and excited states. In the following, we provide two exemplary applications of SA-SF-TDDFT to diradicals.

1. Adiabatic excitation energies

We first examine the performance of SA-SF-TDDFT for adiabatic excitations energies of small carbene-like diradicals. For this, we compare to experimental values[113–117] and to theoretical calculations[56] obtained at the level of equation-of-motion coupled-cluster theory with single and doubles excitations and a noniterative diagonal triples correction [EOM-CCSD(dT)].[118,119] These results are presented in Table V.

We observe an overall trend in which SA-SF-TDDFT clearly outperforms standard SF-TDDFT, with the former affording a MAE of 0.12 eV with respect to the EOM-CCSD(dT) benchmarks, the latter of which are quite close to experimental values (where available). We also observe that singlet–triplet gaps are overestimated in SF-TDDFT, likely due to significant spin contamination. In contrast, SA-SF-TDDFT is inherently free of spin contamination and provides more reliable results.

2. Vertical excitation energies

Next, we examine vertical energy gaps for the lowest electronic states of 1,6-diradicals generated by ring opening in cyclohexane and methylcyclohexane, with unpaired electrons localized on opposite ends of the molecule. Geometries were taken from Ref. 56 and excitation energies from that work are compared to SA-SF-TDDFT values in Table VI.

SA-SF-TDDFT yields a mean absolute error of 0.17 eV whereas standard SF-TDDFT produces a larger error of 0.32 eV. The

TABLE V. Adiabatic excitation energies for small diradicals.

		Error (eV)			
Molecule	State	SF[a]	SA-SF[b]	(dT)[c]	Expt.
CH_2	$^1A_1$	−0.25	0.35	0.42	0.39[d]
CH_2	$^1B_1$	0.86	1.41	1.41	1.43[d]
CH_2	2^1A_1	1.71	2.27	2.53	⋯
NH_2^+	$^1A_1$	0.26	1.36	1.25	1.31[e]
NH_2^+	$^1B_1$	1.02	2.09	1.87	⋯
NH_2^+	2^1A_1	2.04	3.15	3.32	⋯
SiH_2	$^3B_1$	1.31	1.08	0.89	0.91[f]
SiH_2	$^1B_1$	2.12	1.96	1.94	1.02[g]
SiH_2	$^1A_1$	3.44	3.26	3.37	⋯
PH_2^+	$^3B_1$	1.31	0.89	0.79	0.75[h]
PH_2^+	$^1B_1$	2.16	2.04	2.00	1.17[h]
PH_2^+	$^1A_1$	3.59	3.52	3.64	⋯
MAE[i]		0.55	0.12	⋯	

[a]50/50 functional and cc-pVTZ basis set, from Ref. 56.
[b]This work, aug-cc-pVQZ basis set.
[c]EOM-CCSD(dT)/aug-cc-pVQZ, from Ref. 56.
[d]Reference 113.
[e]Reference 114.
[f]Reference 115.
[g]Reference 116.
[h]Reference 117.
[i]MAE with respect to EOM-CCSD(dT) results.

TABLE VI. Vertical excitation energies for three diradicals derived from cyclohexane and methylcyclohexane.

		Excitation energy (eV)		
Molecule	State	SF[a]	SA-SF[b]	(dT)[c]
rC6r	$^3B_1$	1.40	0.81	0.61
	$^1B_1$	2.39	2.32	2.37
	$^1A_1$	5.37	5.27	5.55
rC6Cr	$^3B_1$	1.40	0.82	0.62
	$^1B_1$	2.40	2.33	2.37
	$^1A_1$	5.38	5.28	5.56
rC6rC	$^3B_1$	1.45	0.88	0.70
	$^1B_1$	2.41	2.35	2.38
	$^1A_1$	5.40	5.28	5.55
MAE[d]		0.32	0.17	⋯

[a]50/50 functional and cc-pVTZ basis set, from Ref. 56.
[b]This work, cc-pVTZ basis set.
[c]EOM-SF-CCSD(dT)/6-311G(d), from Ref. 56.
[d]MAE with respect to EOM-CCSD(dT) results.

largest deviations originate from triplet excitation energies, indicating that spin contamination significantly affects the predicted singlet–triplet gaps in the conventional SF-TDDFT approach. This trend is consistent with results presented above, demonstrating improved performance of SA-SF-TDDFT in strongly correlated diradical systems.

H. Singlet–triplet gaps in nitrogen heterocycles

Molecules that violate Hund's rule and exhibit an inverted gap between the lowest singlet excited state (S_1) and the lowest triplet state (T_1), meaning $E(T_1) < E(S_1)$, have attracted attention for design of next-generation organic light-emitting diodes that use thermally activated delayed fluorescence as a means to enhance efficiency.[120,121] Tricyclic nitrogen-containing heterocycles based on cycl[3.3.3]azine ("cyclazine"),[122] including 1,4,7-triazacycl[3.3.3]azine ("heptazine"),[123] have been examined in this context.[46] Several examples that exhibit inverted S_1/T_1 gaps are illustrated in Fig. 20. It has been suggested that S_1/T_1 inversion requires strong coupling between single and double excitations, which cannot be described using conventional LR-TDDFT,[120] and that excited-state KS approach (or "ΔDFT") is preferable to LR-TDDFT for thermally activated delayed fluorescence.[124]

Benchmark $S_0 \rightarrow S_1$ and $S_0 \rightarrow T_1$ transition energies are available for the molecules shown in Fig. 20.[46] Error statistics for TDDFT vertical excitation energies, relative to these benchmarks, are provided in Table S10. In Table VII, these are converted to errors in the S_1/T_1 gap,

$$E_{\text{gap}} = E(S_1) - E(T_1). \tag{17}$$

For the SF methods, these calculations use T_1 as the reference state so that the $T_1 \rightarrow S_n$ $(n = 0, 1)$ transition energies emerge as excitations. For TD-B3LYP, we compute $S_0 \rightarrow S_1$ as an excitation but the $S_0 \rightarrow T_1$ transition energies in Table S10 are from two ground-state calculations.

The TD-B3LYP and SF-TDDFT methods consistently fail to recover the S_1/T_1 inversion, predicting the wrong sign for E_{gap} in all (TD-B3LYP) or nearly all (SF-TDDFT) of the cyclazine derivatives. (A similar observation was recently reported elsewhere.[29]) These methods exhibit MAEs of 0.3–0.4 eV in E_{gap} vs only 0.03 eV for SA-SF-TDDFT, which also predicts the correct sign in every case. Notably, for TD-B3LYP and SF-TDDFT the errors in E_{gap} are larger than the MAEs in the transition energies themselves, which are 0.19 eV in both cases (Table S10).

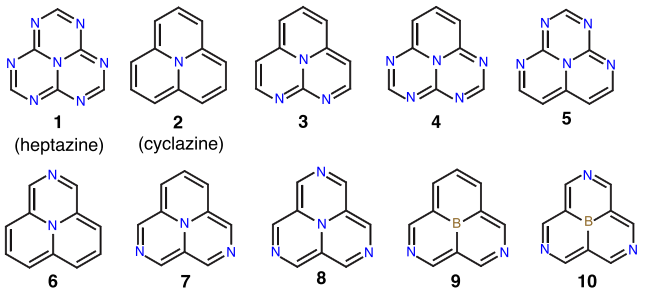

FIG. 20. Cyclazine derivatives with inverted S_1/T_1 gaps, taken from Ref. 46.

TABLE VII. S_1/T_1 gaps in cyclazine derivatives.[a]

	E_{gap} (eV)			
		Spin-flip[d]		
Molecule[b]	TBE[c]	SF	SA-SF	TD-B3LYP
1	−0.22	−0.00	−0.20	0.22
2	−0.13	0.08	−0.15	0.20
3	−0.10	0.20	−0.13	0.27
4	−0.12	0.24	−0.15	0.28
5	−0.10	0.26	−0.11	0.30
6	−0.07	0.20	−0.12	0.25
7	−0.04	0.21	−0.08	0.28
8	−0.03	0.18	−0.05	0.29
9	−0.20	0.13	−0.21	0.21
10	−0.30	−0.41	−0.27	0.11
MAE[e]	⋯	0.26	0.03	0.37

[a] All TDDFT calculations use the aug-cc-pVTZ basis set. See Table S10 for the transition energies.
[b] Numbering corresponds to Fig. 20.
[c] From Ref. 46.
[d] BH&HLYP functional.
[e] Relative to TBE values [Eq. (16)].

IV. CONCLUSION

Our results highlight limitations of conventional TDDFT for systems with strong static correlation such as diradicals, where single-reference methods fail to capture near-degeneracies and often yield spin-contaminated or qualitatively incorrect state ordering. SF-TDDFT, which uses a sacrificial high-spin reference determinant to generate lower-spin states, provides access to multiconfigurational electronic structure at single-reference cost. However, conventional SF-TDDFT is susceptible to spin contamination that can cause substantial errors in vertical excitation energies.

By examining the comprehensive QUEST database,[45] we found—perhaps unexpectedly—that traditional, spin-conserving LR-TDDFT (represented here by the TD-B3LYP approach) often performs better than SF-TDDFT. This is largely a result of spin contamination that degrades the accuracy SF-TDDFT, as may be gleaned by direct comparison to spin-pure SA-SF-TDDFT results using the same functional, namely, BH&HLYP. Across all datasets of QUEST, the SA-SF-TDDFT approach consistently delivers superior accuracy while remaining rigorously free of spin contamination.

Despite these advantages, SA-SF-TDDFT does show limitations for doublet monoradicals in high symmetry (linear or near-linear) geometries. Here, the requisite high-spin quartet reference state affords degenerate or near-degenerate SOMOs, leading to incorrect excitation energies and rendering both SF-TDDFT and SA-SF-TDDFT particularly challenging for such cases. In a sense, the SF approach actually creates a more difficult electron correlation problem in these examples because the spin-flipping excitation must generate two quasi-degenerate determinants. This is likely to be problematic also for open-shell transition metal ions, and work is

in progress to develop new versions of the SF-TDDFT idea that can handle such cases.

This situation leads us to ponder the general nature of static correlation effects in molecular systems, which we suggest can be grouped into three categories. The first are genuinely strong correlation problems, which emerge whenever the gap between occupied and virtual orbitals is $\lesssim$1 eV, such that dynamic electron correlation is enough to prompt a change in electronic configuration. This is the most challenging class of problems but it is a relatively small subset of molecules, at least for closed-shell systems. A second category includes systems with open-shell character and quasi-degenerate SOMOs. Here, it is necessary to treat the open shells appropriately in order to avoid spin contamination that can render spin-unrestricted approaches unreliable. This can be accomplished by augmenting the single-excitation space with a rather limited set of doubly excited determinants, as in SA-SF-TDDFT. Often, this is sufficient to resolve problems with static correlation without the need for a proper multireference description and its associated complexity. This is the realm where properly spin-adapted, open-shell TDDFT methods shine. That being said, we have identified a third case involving doublet radicals with linear or near-linear geometries, which manages to defeat the SA-SF-TDDFT approach because (near-)degeneracies in the high-spin quartet reference state generate a strong correlation problem where one may not have existed previously. Such problems are readily identifiable and can be handled in other ways that maintain single-reference cost, e.g., using the XCIS method. Furthermore, we expect the number of systems in this latter category to be rather small since the presence of substituent moieties is likely to lift degeneracies in the quartet reference state.

The original motivation for developing SF-TDDFT lay in diradicals. For that case, SA-SF-TDDFT provides the most reliable and accurate description among the TDDFT-based approaches considered. Setting aside the special case of (near-)linear monoradicals with (near-)degenerate p_x and p_y orbitals in the quartet reference, our findings demonstrate that SA-SF-TDDFT offers a robust, balanced, and computationally efficient framework for modeling closed and open-shell molecules, outperforming both standard TDDFT and SF-TDDFT in the majority of cases, with a diagnosable failure mechanism in the exceptional cases.

SUPPLEMENTARY MATERIAL

The supplementary material provides the raw data used to make the figures.

ACKNOWLEDGMENTS

This work was supported by the National Science Foundation under Grant No. CHE-2402361.

AUTHOR DECLARATIONS

Conflict of Interest

J.M.H. is part owner of Q-Chem Inc. and serves on its board of directors.

Author Contributions

Avik Kumar Ojha: Data curation (lead); Formal analysis (lead); Investigation (lead); Methodology (supporting); Software (lead); Validation (lead); Writing – original draft (lead); Writing – review & editing (supporting). **John M. Herbert**: Conceptualization (lead); Formal analysis (supporting); Funding acquisition (lead); Methodology (lead); Project administration (lead); Resources (lead); Supervision (lead); Visualization (supporting); Writing – review & editing (lead).

DATA AVAILABILITY

The data that support the findings of this study are available within the article and in the supplementary material.

REFERENCES

[1] J. M. Herbert, "Density-functional theory for electronic excited states," in *Theoretical and Computational Photochemistry: Fundamentals, Methods, Applications and Synergy with Experimental Approaches*, edited by C. García-Iriepa and M. Marazzi (Elsevier, Amsterdam, 2023), Chap. 3, pp. 69–118.
[2] J. M. Herbert, "Visualizing and characterizing excited states from time-dependent density functional theory," Phys. Chem. Chem. Phys. **26**, 3755–3794 (2024).
[3] B. G. Levine, C. Ko, J. Quenneville, and T. J. Martínez, "Conical intersections and double excitations in time-dependent density functional theory," Mol. Phys. **104**, 1039–1051 (2006).
[4] H.-H. Teh and J. E. Subotnik, "The simplest possible approach for simulating S_0–S_1 conical intersections with DFT/TDDFT: Adding *one* doubly excited configuration," J. Phys. Chem. Lett. **10**, 3426–3432 (2019).
[5] V. Athavale, H.-H. Teh, and J. E. Subotnik, "On the inclusion of one double within CIS and TDDFT," J. Chem. Phys. **155**, 154105 (2021).
[6] J. M. Herbert, X. Zhang, A. F. Morrison, and J. Liu, "Beyond time-dependent density functional theory using only single excitations: Methods for computational studies of excited states in complex systems," Acc. Chem. Res. **49**, 931–941 (2016).
[7] J. M. Herbert and A. Mandal, "Spin-flip TDDFT for photochemistry," in *Time-Dependent Density-Functional Theory: Nonadiabatic Molecular Dynamics*, edited by C. Zhu (Jenny Stanford, Singapore, 2023), Chap. 10, pp. 361–404.
[8] Y. Shao, M. Head-Gordon, and A. I. Krylov, "The spin-flip approach within time-dependent density functional theory: Theory and applications to diradicals," J. Chem. Phys. **118**, 4807–4818 (2003).
[9] D. Casanova and A. I. Krylov, "Spin-flip methods in quantum chemistry," Phys. Chem. Chem. Phys. **22**, 4326–4342 (2020).
[10] S. Lee, W. Park, and C. H. Choi, "Expanding horizons in quantum chemical studies: The versatile power of MRSF-TDDFT," Acc. Chem. Res. **58**, 208–217 (2025).
[11] Y. Harabuchi, S. Maeda, T. Taketsugu, N. Minezawa, and K. Morokuma, "Automated search for minimum energy conical intersection geometries between the lowest two singlet states S_0/S_1-MECIs by the spin-flip TDDFT method," J. Chem. Theory Comput. **9**, 4116–4123 (2013).
[12] S. Maeda, Y. Harabuchi, T. Taketsugu, and K. Morokuma, "Systematic exploration of minimum energy conical intersection structures near the Franck–Condon region," J. Phys. Chem. A **118**, 12050–12058 (2014).
[13] X. Zhang and J. M. Herbert, "Analytic derivative couplings in time-dependent density functional theory: Quadratic response theory versus pseudo-wavefunction approach," J. Chem. Phys. **142**, 064109 (2015).
[14] X. Zhang and J. M. Herbert, "Analytic derivative couplings for spin-flip configuration interaction singles and spin-flip time-dependent density functional theory," J. Chem. Phys. **141**, 064104 (2014).
[15] X. Zhang and J. M. Herbert, "Excited-state deactivation pathways in uracil versus hydrated uracil: Solvatochromatic shift in the $^1n\pi^*$ state is the key," J. Phys. Chem. B **118**, 7806–7817 (2014).

[16]N. Minezawa and M. S. Gordon, "Photoisomerization of stilbene: A spin-flip density functional theory study," J. Phys. Chem. A **115**, 7901–7911 (2011).
[17]N. Minezawa and M. S. Gordon, "Optimizing conical intersections of solvated molecules: The combined spin-flip density functional theory/effective fragment potential method," J. Chem. Phys. **137**, 034116 (2012).
[18]Y. Harabuchi, K. Keipert, F. Zahariev, T. Taketsugu, and M. S. Gordon, "Dynamics simulations with spin-flip time-dependent density functional theory: Photoisomerization and photocyclization mechanisms of *cis*-stilbene in $\pi\pi^*$ states," J. Phys. Chem. A **118**, 11987–11998 (2014).
[19]L. Yue, Z. Lan, and Y.-J. Liu, "The theoretical estimation of the bioluminescent efficiency of the firefly via a nonadiabatic molecular dynamics simulation," J. Phys. Chem. Lett. **6**, 540–548 (2015).
[20]X. Zhang and J. M. Herbert, "Nonadiabatic dynamics with spin-flip versus linear-response time-dependent density functional theory: A case study for the protonated Schiff base $C_5H_6NH_2^+$," J. Chem. Phys. **155**, 124111 (2021).
[21]T. Taketsugu, T. Tsutsumi, Y. Harabuchi, and T. Tsuneda, "On-the-fly excited-state molecular dynamics study based on spin-flip time-dependent density functional theory approach: Photo-branching reaction of stilbene and stilbene derivatives," in *Time-Dependent Density-Functional Theory: Nonadiabatic Molecular Dynamics*, edited by C. Zhu (Jenny Stanford, Singapore, 2023), Chap. 2, pp. 39–73.
[22]A. I. Krylov, "Size-consistent wave functions for bond-breaking: The equation-of-motion spin-flip model," Chem. Phys. Lett. **338**, 375–384 (2001).
[23]Y. Horbatenko, S. Sadiq, S. Lee, M. Filatov, and C. H. Choi, "Mixed-reference spin-flip time-dependent density functional theory (MRSF-TDDFT) as a simple yet accurate method for diradicals and diradicaloids," J. Chem. Theory Comput. **17**, 848–859 (2021).
[24]X. Zhang and J. M. Herbert, "Spin-flip, tensor equation-of-motion configuration interaction with a density-functional correction: A spin-complete method for exploring excited-state potential energy surfaces," J. Chem. Phys. **143**, 234107 (2015).
[25]Z. Li and W. Liu, "Spin-adapted open-shell random phase approximation and time-dependent density functional theory. I. Theory," J. Chem. Phys. **133**, 064106 (2010).
[26]Z. Li, W. Liu, Y. Zhang, and B. Suo, "Spin-adapted open-shell time-dependent density functional theory. II. Theory and pilot application," J. Chem. Phys. **134**, 134101 (2011).
[27]Z. Li and W. Liu, "Spin-adapted open-shell time-dependent density functional theory. III. An even better and simpler formulation," J. Chem. Phys. **135**, 194106 (2011).
[28]Z. Wang, Z. Li, Y. Zhang, and W. Liu, "Analytic energy gradients of spin-adapted open-shell time-dependent density functional theory," J. Chem. Phys. **153**, 164109 (2020).
[29]H. Zhao and Z. Li, "Spin-adapted open-shell time-dependent density functional theory: Towards a simple and accurate method for spin-flip-down excitations," Mol. Phys. (published online 2026).
[30]D. J. Rowe and C. Ngo-Trong, "Tensor equations of motion for the excitations of rotationally invariant or charge-independent systems," Rev. Mod. Phys. **47**, 471–485 (1975).
[31]S. Grimme, "Density functional calculations with configuration interaction for the excited states of molecules," Chem. Phys. Lett. **259**, 128–137 (1996).
[32]A. Mandal, E. J. Berquist, and J. M. Herbert, "A new parameterization of the DFT/CIS method with applications to core-level spectroscopy," J. Chem. Phys. **161**, 044114 (2024).
[33]A. Mandal and J. M. Herbert, "Computing L- and M-edge spectra using the DFT/CIS method with spin–orbit coupling," Phys. Chem. Chem. Phys. **27**, 16336–16353 (2025).
[34]K. Yang, R. Peverati, D. G. Truhlar, and R. Valero, "Density functional study of multiplicity-changing valence and Rydberg excitations of p-block elements: Delta self-consistent field, collinear spin-flip time-dependent density functional theory (DFT), and conventional time-dependent DFT," J. Chem. Phys. **135**, 044118 (2011).
[35]Z. Li and W. Liu, "Theoretical and numerical assessments of spin-flip time-dependent density functional theory," J. Chem. Phys. **136**, 024107 (2012).
[36]M. Isegawa and D. G. Truhlar, "Valence excitation energies of alkenes, carbonyl compounds, and azabenzenes by time-dependent density functional theory: Linear response of the ground state compared to collinear and noncollinear spin-flip TDDFT with the Tamm-Dancoff approximation," J. Chem. Phys. **138**, 134111 (2013).
[37]X. Xu, K. R. Yang, and D. G. Truhlar, "Testing noncollinear spin-flip, collinear spin-flip, and conventional time-dependent density functional theory for predicting electronic excitation energies of closed-shell atoms," J. Chem. Theory Comput. **10**, 2070–2084 (2014).
[38]N. Minezawa, "Vertical excitation energies of linear cyanine dyes by spin-flip time-dependent density functional theory," Chem. Phys. Lett. **622**, 115–119 (2015).
[39]S. Lee, S. Shostak, M. Filatov, and C. H. Choi, "Conical intersections in organic molecules: Benchmarking mixed-reference spin–flip time-dependent DFT (MSRF-TD-DFT) vs spin–flip TD-DFT," J. Phys. Chem. A **123**, 6455–6462 (2019).
[40]Y. Horbatenko, S. Lee, M. Filatov, and C. H. Choi, "Performance analysis and optimization of mixed-reference spin-flip time-dependent density functional theory (MRSF-TDDFT) for vertical excitation energies and singlet–triplet energy gaps," J. Phys. Chem. A **123**, 7991–8000 (2019).
[41]S. Lee, M. Filatov, S. Lee, and C. H. Choi, "Eliminating spin-contamination of spin-flip time dependent density functional theory within linear response formalism by the use of zeroth-order mixed-reference (MR) reduced density matrix," J. Chem. Phys. **149**, 104101 (2018).
[42]Y. Horbatenko, S. Lee, M. Filatov, and C. H. Choi, "How beneficial is the *explicit* account of doubly-excited configurations in linear response theory?," J. Chem. Theory Comput. **17**, 975–984 (2021).
[43]S. Lee, W. Park, H. Nakata, M. Filatov, and C. H. Choi, "Mixed-reference spin-flip time-dependent density functional theory (MRSF-TDDFT) as a method of choice for nonadiabatic molecular dynamics," in *Time-Dependent Density-Functional Theory: Nonadiabatic Molecular Dynamics*, edited by C. Zhu (Jenny Stanford, Singapore, 2023), Chap. 4, pp. 101–139.
[44]B. Suo, K. Shen, Z. Li, and W. Liu, "Performance of TD-DFT for excited states of open-shell transition metal compounds," J. Phys. Chem. A **121**, 3929–3942 (2017).
[45]M. Véril, A. Scemama, M. Caffarel, F. Lipparini, M. Boggio-Pasqua, D. Jacquemin, and P.-F. Loos, "QUESTDB: A database of highly accurate excitation energies for the electronic structure community," Wiley Interdiscip. Rev.: Comput. Mol. Sci. **11**, e1517 (2021).
[46]P.-F. Loos, F. Lipparini, and D. Jacquemin, "Heptazine, cyclazine, and related compounds: Chemically-accurate estimates of the inverted singlet–triplet gap," J. Phys. Chem. Lett. **14**, 11069–11075 (2023).
[47]D. W. Small, E. J. Sundstrom, and M. Head-Gordon, "A simple way to test for collinearity in spin symmetry broken wave functions: General theory and application to generalized Hartree Fock," J. Chem. Phys. **142**, 094112 (2015).
[48]H. Li, Z. Pu, Q. Sun, Y. Q. Gao, and Y. Xiao, "Noncollinear and spin-flip TDDFT in multicollinear approach," J. Chem. Theory Comput. **19**, 2270–2281 (2023).
[49]F. Wang and W. Liu, "Comparison of different polarization schemes in open-shell relativistic density functional calculations," J. Chin. Chem. Soc. **50**, 597–606 (2003).
[50]J. Gao, W. Liu, B. Song, and C. Liu, "Time-dependent four-component relativistic density functional theory for excitation energies," J. Chem. Phys. **121**, 6658–6666 (2004).
[51]J. Gao, W. Zou, W. Liu, Y. Xiao, D. Peng, B. Song, and C. Liu, "Time-dependent four-component relativistic density-functional theory for excitation energies. II. The exchange-correlation kernel," J. Chem. Phys. **123**, 054102 (2005).
[52]F. Wang and T. Ziegler, "Time-dependent density functional theory based on a noncollinear formulation of the exchange-correlation potential," J. Chem. Phys. **121**, 12191 (2004).
[53]F. Wang and T. Ziegler, "The performance of time-dependent density functional theory based on a noncollinear exchange-correlation potential in the calculations of excitation energies," J. Chem. Phys. **122**, 074109 (2005).
[54]Z. Rinkevicius and H. Ågren, "Spin-flip time dependent density functional theory for singlet–triplet splittings in σ,σ-biradicals," Chem. Phys. Lett. **491**, 132–135 (2010).

[55]Z. Rinkevicius, O. Vahtras, and H. Ågren, "Spin-flip time dependent density functional theory applied to excited states with single, double, or mixed electron excitation character," J. Chem. Phys. **133**, 114104 (2010).
[56]Y. A. Bernard, Y. Shao, and A. I. Krylov, "General formulation of spin-flip time-dependent density functional theory using non-collinear kernels: Theory, implementation, and benchmarks," J. Chem. Phys. **136**, 204103 (2012).
[57]C. S. Chibueze and L. Visscher, "Spin-adapted spin-flip-down time-dependent density functional theory," J. Chem. Phys. **163**, 094111 (2025).
[58]M. Huix-Rotllant, B. Natarajan, A. Ipatov, C. Muhavini Wawire, T. Deutsch, and M. E. Casida, "Assessment of noncollinear spin-flip Tamm–Dancoff approximation time-dependent density-functional theory for the photochemical ring-opening of oxirane," Phys. Chem. Chem. Phys. **12**, 12811–12825 (2010).
[59]S. Komorovsky, P. J. Cherry, and M. Repisky, "Four-component relativistic time-dependent density-functional theory using a stable noncollinear DFT ansatz applicable to both closed- and open-shell systems," J. Chem. Phys. **151**, 184111 (2019).
[60]L. I. Hernandez-Segura and S. Luber, "Spin-flip TDDFT within the Sternheimer formulation: A Gaussian and plane wave implementation," J. Phys. Chem. A **129**, 9798–9809 (2025).
[61]H. Li, Q. Sun, Y. Q. Gao, and Y. Xiao, "Analytic gradient for spin-flip TDDFT using noncollinear functionals in the multicollinear approach," J. Chem. Theory Comput. **21**, 3010–3031 (2025).
[62]F. Furche, "On the density matrix based approach to time-dependent density functional response theory," J. Chem. Phys. **114**, 5982–5992 (2001).
[63]M. Gray, A. Mandal, and J. M. Herbert, "Revisiting the half-and-half functional," J. Phys. Chem. A **129**, 3969–3982 (2025).
[64]K. D. Closser, O. Gessner, and M. Head-Gordon, "Simulations of the dissociation of small helium clusters with *ab initio* molecular dynamics in electronically excited states," J. Chem. Phys. **140**, 134306 (2014).
[65]C. M. Marian, A. Heil, and M. Kleinschmidt, "The DFT/MRCI method," Wiley Interdiscip. Rev.: Comput. Mol. Sci. **9**, e1394 (2018).
[66]E. Epifanovsky, A. T. B. Gilbert, X. Feng, J. Lee, Y. Mao, N. Mardirossian, P. Pokhilko, A. F. White, M. P. Coons, A. L. Dempwolff, Z. Gan, D. Hait, P. R. Horn, L. D. Jacobson, I. Kaliman, J. Kussmann, A. W. Lange, K. U. Lao, D. S. Levine, J. Liu, S. C. McKenzie, A. F. Morrison, K. D. Nanda, F. Plasser, D. R. Rehn, M. L. Vidal, Z.-Q. You, Y. Zhu, B. Alam, B. J. Albrecht, A. Aldossary, E. Alguire, J. H. Andersen, V. Athavale, D. Barton, K. Begam, A. Behn, N. Bellonzi, Y. A. Bernard, E. J. Berquist, H. G. A. Burton, A. Carreras, K. Carter-Fenk, R. Chakraborty, A. D. Chien, K. D. Closser, V. Cofer-Shabica, S. Dasgupta, M. de Wergifosse, J. Deng, M. Diedenhofen, H. Do, S. Ehlert, P.-T. Fang, S. Fatehi, Q. Feng, T. Friedhoff, J. Gayvert, Q. Ge, G. Gidofalvi, M. Goldey, J. Gomes, C. E. González-Espinoza, S. Gulania, A. O. Gunina, M. W. D. Hanson-Heine, P. H. P. Harbach, A. Hauser, M. F. Herbst, M. Hernández Vera, M. Hodecker, Z. C. Holden, S. Houck, X. Huang, K. Hui, B. C. Huynh, M. Ivanov, Á. Jász, H. Ji, H. Jiang, B. Kaduk, S. Kähler, K. Khistyaev, J. Kim, G. Kis, P. Klunzinger, Z. Koczor-Benda, J. H. Koh, D. Kosenkov, L. Koulias, T. Kowalczyk, C. M. Krauter, K. Kue, A. Kunitsa, T. Kus, I. Ladjánszki, A. Landau, K. V. Lawler, D. Lefrancois, S. Lehtola, R. R. Li, Y.-P. Li, J. Liang, M. Liebenthal, H.-H. Lin, Y.-S. Lin, F. Liu, K.-Y. Liu, M. Loipersberger, A. Luenser, A. Manjanath, P. Manohar, E. Mansoor, S. F. Manzer, S.-P. Mao, A. V. Marenich, T. Markovich, S. Mason, S. A. Maurer, P. F. McLaughlin, M. F. S. J. Menger, J.-M. Mewes, S. A. Mewes, P. Morgante, J. W. Mullinax, K. J. Oosterbaan, G. Paran, A. C. Paul, S. K. Paul, F. Pavošević, Z. Pei, S. Prager, E. I. Proynov, Á. Rák, E. Ramos-Cordoba, B. Rana, A. E. Rask, A. Rettig, R. M. Richard, F. Rob, E. Rossomme, T. Scheele, M. Scheurer, M. Schneider, N. Sergueev, S. M. Sharada, W. Skomorowski, D. W. Small, C. J. Stein, Y.-C. Su, E. J. Sundstrom, Z. Tao, J. Thirman, G. J. Tornai, T. Tsuchimochi, N. M. Tubman, S. P. Veccham, O. Vydrov, J. Wenzel, J. Witte, A. Yamada, K. Yao, S. Yeganeh, S. R. Yost, A. Zech, I. Y. Zhang, X. Zhang, Y. Zhang, D. Zuev, A. Aspuru-Guzik, A. T. Bell, N. A. Besley, K. B. Bravaya, B. R. Brooks, D. Casanova, J.-D. Chai, S. Coriani, C. J. Cramer, G. Cserey, A. E. DePrince III, R. A. DiStasio, Jr., A. Dreuw, B. D. Dunietz, T. R. Furlani, W. A. Goddard III, S. Hammes-Schiffer, T. Head-Gordon, W. J. Hehre, C.-P. Hsu, T.-C. Jagau, Y. Jung, A. Klamt, J. Kong, D. S. Lambrecht, W. Liang, N. J. Mayhall, C. W. McCurdy, J. B. Neaton, C. Ochsenfeld, J. A. Parkhill, R. Peverati, V. A. Rassolov, Y. Shao, L. V. Slipchenko, T. Stauch, R. P. Steele, J. E. Subotnik, A. J. W. Thom, A. Tkatchenko, D. G. Truhlar, T. Van Voorhis, T. A. Wesolowski, K. B. Whaley, H. L. Woodcock III, P. M. Zimmerman, S. Faraji, P. M. W. Gill, M. Head-Gordon, J. M. Herbert, and A. I. Krylov, "Software for the frontiers of quantum chemistry: An overview of developments in the Q-Chem 5 package," J. Chem. Phys. **155**, 084801 (2021).
[67]G. M. J. Barca, C. Bertoni, L. Carrington, D. Datta, N. De Silva, J. E. Deustua, D. G. Fedorov, J. R. Gour, A. O. Gunina, E. Guidez, T. Harville, S. Irle, J. Ivanic, K. Kowalski, S. S. Leang, H. Li, W. Li, J. J. Lutz, I. Magoulas, J. Mato, V. Mironov, H. Nakata, B. Q. Pham, P. Piecuch, D. Poole, S. R. Pruitt, A. P. Rendell, L. B. Roskop, K. Ruedenberg, T. Sattasathuchana, M. W. Schmidt, J. Shen, L. Slipchenko, M. Sosonkina, V. Sundriyal, A. Tiwari, J. L. Galvez Vallejo, B. Westheimer, M. Włoch, P. Xu, F. Zahariev, and M. S. Gordon, "Recent developments in the general atomic and molecular electronic structure system," J. Chem. Phys. **152**, 154102 (2020).
[68]J. Liang, X. Feng, D. Hait, and M. Head-Gordon, "Revisiting the performance of time-dependent density functional theory for electronic excitations: Assessment of 43 popular and recently developed functionals from rungs one to four," J. Chem. Theory Comput. **18**, 3460–3473 (2022).
[69]P. M. W. Gill, B. G. Johnson, and J. A. Pople, "A standard grid for density-functional calculations," Chem. Phys. Lett. **209**, 506–512 (1993).
[70]S. Dasgupta and J. M. Herbert, "Standard grids for high-precision integration of modern density functionals: SG-2 and SG-3," J. Comput. Chem. **38**, 869–882 (2017).
[71]B. N. Plakhutin and E. R. Davidson, "Canonical form of the Hartree-Fock orbitals in open-shell systems," J. Chem. Phys. **140**, 014102 (2014).
[72]A. K. Ojha and J. M. Herbert, "Extended configuration-interaction singles method with core/valence separation (XCIS-CVS): Core-level spectra of open-shell molecules," J. Chem. Theory Comput. **21**, 12172–12184 (2025).
[73]P.-F. Loos, A. Scemama, M. Boggio-Pasqua, and D. Jacquemin, "Mountaineering strategy to excited states: Highly accurate energies and benchmarks for exotic molecules and radicals," J. Chem. Theory Comput. **16**, 3720–3736 (2020).
[74]P.-F. Loos, M. Boggio-Pasqua, A. Blondel, F. Lipparini, and D. Jacquemin, "QUEST database of highly-accurate excitation energies," J. Chem. Theory Comput. **21**, 8010–8033 (2025).
[75]P.-F. Loos, A. Scemama, A. Blondel, Y. Garniron, M. Caffarel, and D. Jacquemin, "A mountaineering strategy to excited states: Highly accurate reference energies and benchmarks," J. Chem. Theory Comput. **14**, 4360–4379 (2018).
[76]J. Fabian, "Electronic excitation of sulfur-organic compounds – performance of time-dependent density functional theory," Theor. Chim. Acta **106**, 199–217 (2001).
[77]M. Schreiber, V. Buß, and M. P. Fülscher, "The electronic spectra of symmetric cyanine dyes: A CASPT2 study," Phys. Chem. Chem. Phys. **3**, 3906–3912 (2001).
[78]A. E. Masunov, "Theoretical spectroscopy of carbocyanine dyes made accurate by frozen density correction to excitation energies obtained by TD-DFT," Int. J. Quantum Chem. **110**, 3095–3100 (2010).
[79]B. Moore II and J. Autschbach, "Longest-wavelength electronic excitations of linear cyanines: The role of electron delocalization and of approximations in time-dependent density functional theory," J. Chem. Theory Comput. **9**, 4991–5003 (2013).
[80]H. Zhekova, M. Krykunov, J. Autschbach, and T. Ziegler, "Applications of time dependent and time independent density functional theory to the first π and π^* transition in cyanine dyes," J. Chem. Theory Comput. **10**, 3299–3307 (2014).
[81]P. Boulanger, D. Jacquemin, I. Duchemin, and X. Blase, "Fast and accurate electronic excitations in cyanines with the many-body Bethe–Salpeter approach," J. Chem. Theory Comput. **10**, 1212–1218 (2014).
[82]D. Jacquemin, S. Chibani, B. Le Guennic, and B. Mennucci, "Solvent effects on cyanine derivatives: A PCM investigation," J. Phys. Chem. A **118**, 5343–5348 (2014).
[83]B. Le Guennic and D. Jacquemin, "Taking up the cyanine challenge with quantum tools," Acc. Chem. Res. **48**, 530–537 (2015).
[84]P.-F. Loos, F. Lipparini, M. Boggio-Pasqua, A. Scemama, and D. Jacquemin, "A mountaineering strategy to excited states: Highly accurate energies and benchmarks for medium sized molecules," J. Chem. Theory Comput. **16**, 1711–1741 (2020).
[85]S. Grimme and F. Neese, "Double-hybrid density functional theory for excited electronic states of molecules," J. Chem. Phys. **127**, 154116 (2007).
[86]W. Helal, "Double hybrid density functionals for the electronic excitation energies of linear cyanines," J. Phys. Chem. A **127**, 131–141 (2023).

[87]D. Jacquemin, Y. Zhao, R. Valero, C. Adamo, I. Ciofini, and D. G. Truhlar, "Verdict: Time-dependent density functional theory 'not guilty' of large errors for cyanines," J. Chem. Theory Comput. **8**, 1255–1259 (2012).
[88]R. Send, O. Valsson, and C. Filippi, "Electronic excitations of simple cyanine dyes: Reconciling density functional and wave function methods," J. Chem. Theory Comput. **7**, 444–455 (2011).
[89]Q. Ou, Q. Peng, and Z. Shuai, "Toward quantitative prediction of fluorescence quantum efficiency by combining direct vibrational conversion and surface crossing: BODIPYs as an example," J. Phys. Chem. Lett. **11**, 7790–7797 (2020).
[90]S. Chibani, B. Le Guennic, A. Charaf-Eddin, A. D. Laurent, and D. Jacquemin, "Revisiting the optical signatures of BODIPY with *ab initio* tools," Chem. Sci. **4**, 1950–1963 (2013).
[91]A. Charaf-Eddin, B. Le Guennic, and D. Jacquemin, "Excited-states of BODIPY–cyanines: Ultimate TD-DFT challenges?," RSC Adv. **4**, 49449–49456 (2014).
[92]S. Chibani, A. D. Laurent, B. Le Guennic, and D. Jacquemin, "Improving the accuracy of excited-state simulations of BODIPY and aza-BOPDIPY dyes with a joint SOS-CIS(D) and TD-DFT approach," J. Chem. Theory Comput. **10**, 4574–4582 (2014).
[93]M. R. Momeni and A. Brown, "Why do TD-DFT excitation energies of BODIPY/aza-BODIPY families largely deviate from experiment? Answers from electron correlated and multireference methods," J. Chem. Theory Comput. **11**, 2619–2632 (2015).
[94]Z. Lin, A. W. Kohn, and T. Van Voorhis, "Toward prediction of nonradiative decay pathways in organic compounds II: Two internal conversion channels in BODIPYs," J. Phys. Chem. C **124**, 3925–3938 (2020).
[95]P.-F. Loos, M. Comin, X. Blase, and D. Jacquemin, "Reference energies for intramolecular charge-transfer excitations," J. Chem. Theory Comput. **17**, 3666–3686 (2021).
[96]A. W. Lange, M. A. Rohrdanz, and J. M. Herbert, "Charge-transfer excited states in a π-stacked adenine dimer, as predicted using long-range-corrected time-dependent density functional theory," J. Phys. Chem. B **112**, 6304–6308 (2008).
[97]M. A. Rohrdanz and J. M. Herbert, "Simultaneous benchmarking of ground- and excited-state properties with long-range-corrected density functional theory," J. Chem. Phys. **129**, 034107 (2008).
[98]B. Alam, A. F. Morrison, and J. M. Herbert, "Charge separation and charge transfer in the low-lying excited states of pentacene," J. Phys. Chem. C **124**, 24653–24666 (2020).
[99]M. A. Rohrdanz, K. M. Martins, and J. M. Herbert, "A long-range-corrected density functional that performs well for both ground-state properties and time-dependent density functional theory excitation energies, including charge-transfer excited states," J. Chem. Phys. **130**, 054112 (2009).
[100]A. W. Lange and J. M. Herbert, "Both intra- and interstrand charge-transfer excited states in B-DNA are present at energies comparable to, or just above, the $^1\pi\pi^*$ excitonic bright states," J. Am. Chem. Soc. **131**, 3913–3922 (2009).
[101]M. Modrzejewski, Ł. Rajchel, G. Chalasinski, and M. M. Szczesniak, "Density-dependent onset of the long-range exchange: A key to donor–acceptor properties," J. Phys. Chem. A **117**, 11580–11586 (2013).
[102]A. Mandal and J. M. Herbert, "Simplified tuning of long-range corrected time-dependent density functional theory," J. Phys. Chem. Lett. **16**, 2672–2680 (2025).
[103]A. Dreuw, J. L. Weisman, and M. Head-Gordon, "Long-range charge-transfer excited states in time-dependent density functional theory require non-local exchange," J. Chem. Phys. **119**, 2943–2946 (2003).
[104]P.-F. Loos and D. Jacquemin, "A mountaineering strategy to excited states: Highly accurate energies and benchmarks for bicyclic systems," J. Phys. Chem. A **125**, 10174–10188 (2021).
[105]J. M. Herbert and A. Mandal, "Importance of orbital invariance in quantifying electron–hole separation and exciton size," J. Chem. Theory Comput. **20**, 9446–9463 (2024).
[106]A. Lange and J. M. Herbert, "Simple methods to reduce charge-transfer contamination in time-dependent density-functional calculations of clusters and liquids," J. Chem. Theory Comput. **3**, 1680–1690 (2007).
[107]R. M. Richard and J. M. Herbert, "Time-dependent density-functional description of the ^1L_a state in polycyclic aromatic hydrocarbons: Charge-transfer character in disguise?," J. Chem. Theory Comput. **7**, 1296–1306 (2011).
[108]D. Dunlop, L. Ludvíková, A. Banerjee, H. Ottosson, and T. Slanina, "Excited-state (anti)aromaticity explains why azulene disobeys Kasha's rule," J. Am. Chem. Soc. **145**, 21569–21575 (2023).
[109]X. Zhang, T. Wang, Y. Q. Gao, and Y. Xiao, "Noncollinear spin-flip TDDFT for potential energy surface crossings: Conical intersections and spin crossings," J. Chem. Theory Comput. **21**, 11550–11561 (2025).
[110]D. Maurice and M. Head-Gordon, "On the nature of electronic transitions in radicals: An extended single excitation configuration interaction method," J. Phys. Chem. **100**, 6131–6137 (1996).
[111]M. Seth and T. Ziegler, "Calculation of excitation energies of open-shell molecules with spatially degenerate ground states. I. Transformed reference via an intermediate configuration Kohn-Sham density-functional theory and applications to d^1 and d^2 systems with octahedral and tetrahedral symmetries," J. Chem. Phys. **123**, 144105 (2005).
[112]F. G. Eich, S. Pittalis, and G. Vignale, "Transverse and longitudinal gradients of the spin magnetization in spin-density-functional theory," Phys. Rev. B **88**, 245102 (2013).
[113]P. Jensen and P. R. Bunker, "The potential surface and stretching frequencies of $\tilde{X}\,^3B_1$ methylene (CH_2) determined from experiment using the Morse oscillator-rigid bender internal dynamics Hamiltonian," J. Chem. Phys. **89**, 1327–1332 (1988).
[114]S. T. Gibson, J. P. Green, and J. Berkowitz, "Photoionization of the amidogen radical," J. Chem. Phys. **83**, 4319–4328 (1985).
[115]J. Berkowitz, J. P. Greene, H. Cho, and B. Ruščić, "Photoionization mass spectrometric studies of SiH_n (n = 1–4)," J. Chem. Phys. **86**, 1235–1248 (1987).
[116]R. Escribano and A. Campargue, "Absorption spectroscopy of SiH_2 near 640 nm," J. Chem. Phys. **108**, 6249–6257 (1998).
[117]J. Berkowitz and H. Cho, "A photoionization study of PH: PH_2 revisited," J. Chem. Phys. **90**, 1–6 (1989).
[118]M. W. Łoch, M. D. Lodriguito, P. Piecuch, and J. R. Gour, "Two new classes of non-iterative coupled-cluster methods derived from the method of moments of coupled-cluster equations," Mol. Phys. **104**, 2149–2172 (2006).
[119]P. U. Manohar and A. I. Krylov, "A noniterative perturbative triples correction for the spin-flipping and spin-conserving equation-of-motion coupled-cluster methods with single and double substitutions," J. Chem. Phys. **129**, 194105 (2008).
[120]P. de Silva, "Inverted singlet–triplet gaps and their relevance to thermally activated delayed fluorescence," J. Phys. Chem. Lett. **10**, 5674–5679 (2019).
[121]G. Ricci, J.-C. Sancho-García, and Y. Olivier, "Establishing design strategies for emissive materials with an inverted singlet–triplet energy gap (INVEST): A computational perspective on how symmetry rules the interplay between triplet harvesting and light emission," J. Mater. Chem. C **10**, 12680–12698 (2022).
[122]W. Leupin and J. Wirz, "Low-lying electronically excited states of cycl[3.3.3]azine, a bridged 12π-perimeter," J. Am. Chem. Soc. **102**, 6068–6075 (1980).
[123]W. Leupin, D. Magde, G. Persy, and J. Wirz, "1,4,7-triazacycl[3.3.3]azine: Basicity, photoelectron spectrum, photophysical properties," J. Am. Chem. Soc. **108**, 17–22 (1986).
[124]T. Froitzheim, L. Kunze, S. Grimme, J. M. Herbert, and J.-M. Mewes, "Benchmarking charge-transfer excited states in TADF emitters: ΔDFT outperforms TD-DFT for emission energies," J. Phys. Chem. A **128**, 6324–6335 (2024).